Title: 3D Mitochondrial Structure in Aging Human Skeletal Muscle: Insights into MFN-2 Mediated Changes

Authors and Affiliations:

Estevao Scudese[1,2,3]*, Zer Vue[1]*, Prassana Katti[4*], Andrea Marshall[1], Larry Vang[1], Edgar Garza López[5], Kit Neikirk[1], Dominique Stephens[1], Duane D. Hall[5], Rahmati Rostami[6], Jian-qiang Shao[7], Margaret Mungai[1], Salma T. AshShareef[5], Innes Hicsasmaz[5], Sasha Manus[1], Celestine Wanjalla[8], Aaron Whiteside[1,9], Clintoria Williams[9], Steven M. Damo[10], Jennifer A. Gaddy[11,12], Annet Kirabo[13], Brian Glancy[4,14], Estélio Henrique Martin Dantas[2,15,16,17,18], André Kinder[19], Fabiana Scartoni[2], Matheus Baffi[3], Melanie R. McReynolds[20], Mark A. Phillips[21], Vernat Exil[22], Bret C. Mobley[23]#, Antentor Hinton[1]#

[1] Department of Molecular Physiology and Biophysics, Vanderbilt University, Nashville, TN, 37232, USA

[2] Laboratory of Biosciences of Human Motricity (LABIMH) of the Federal University of State of Rio de Janeiro (UNIRIO), Rio de Janeiro, Brazil

[3] Sport Sciences and Exercise Laboratory (LaCEE), Catholic University of Petrópolis (UCP), Brazil

[4] National Heart, Lung, and Blood Institute, National Institutes of Health, Bethesda, MD, 20892, USA

[5] Department of Internal Medicine, University of Iowa, Iowa City, IA, 52242, USA

[6] Department of Genetic Medicine, Joan & Sanford I. Weill Medical College of Cornell University, New York, NY, 10065, USA

[7] Central Microscopy Research Facility, Iowa City, IA 52242, USA

[8] Division of Infection Diseases, Department of Medicine, Vanderbilt University Medical Center, Nashville, TN, 37232, USA

[9] Department of Neuroscience, Cell Biology and Physiology, Wright State University, Dayton, OH, 45435, USA

[10] Department of Life and Physical Sciences, Fisk University, Nashville, TN, 37208, USA

[11] Department of Medicine, Vanderbilt University Medical Center, Nashville, TN, 37232, USA

[12] Tennessee Valley Healthcare Systems, U.S. Department of Veterans Affairs, Nashville, TN, 37212, USA

[13] Department of Medicine, Vanderbilt University Medical Center, Nashville, Tennessee, USA

[14] NIAMS, NIH, Bethesda, MD, 20892, USA

[15] Doctor's Degree Program in Nursing and Biosciences - PpgEnfBio, Federal University of the State of Rio de Janeiro - UNIRIO, Rio de Janeiro, RJ, Brazil

[16] Laboratory of Human Motricity Biosciences - LABIMH, Federal University of the State of Rio de Janeiro - UNIRIO, RJ, Brazil

[17] Brazilian Paralympic Academy – APB

[18] Doctor's Degree Program in Health and Environment - PSA, Tiradentes University - UNIT, Aracaju, SE, Brazil

[19] Artur Sá Earp Neto University Center - UNIFASE-FMP, Petrópolis Medical School, Brazil

[20] Department of Biochemistry and Molecular Biology, The Huck Institute of the Life Sciences, Pennsylvania State University, State College, PA, 16801, USA

[21] Department of Integrative Biology, Oregon State University, Corvallis, OR, 97331, USA

[22] Department of Pediatrics, Div. of Cardiology, St. Louis University School of Medicine, St. Louis, MO, 63104, USA

[23] Department of Pathology, Vanderbilt University Medical Center, Nashville, TN, 37232, USA

*These authors share co-first authorship.

#These authors share senior authorship.

Corresponding Author:

Antentor Hinton

Department of Molecular Physiology and Biophysics
Vanderbilt University
antentor.o.hinton.jr@Vanderbilt.Edu 319-383-3095

Keywords: Mitochondria, Sarcopenia, Exercise, Human Skeletal Muscle, 3D Reconstruction, MFN2

Abstract: Sarcopenia is an age-related loss of skeletal muscle, characterized by loss of mass, strength, endurance, and oxidative capacity during aging. Notably, bioenergetics and protein turnover studies have shown that mitochondria mediate this decline in function. Although mitochondrial aging is associated with endoplasmic reticulum stress, fragmented mitochondria, and decreased mitochondrial capacity, the three-dimensional (3D) mitochondrial structure associated with morphological changes in skeletal muscle during aging still requires further elucidation. Moreover, the mechanisms by which 3D mitochondrial networks and mitochondrial specialization are altered during aging are not completely understood. Although exercise has been the only therapy to mitigate sarcopenia, the mechanisms that govern these changes remain unclear. We hypothesized that aging causes structural remodeling of mitochondrial 3D architecture representative of dysfunction, and this effect is mitigated by exercise. We used serial block-face scanning electron microscopy to image human skeletal tissue samples, followed by manual contour tracing using Amira software for 3D reconstruction and subsequent analysis of mitochondria. We then applied a rigorous *in vitro* and *in vivo* exercise regimen during aging. We found that mitochondria became less complex with age. Specifically, mitochondria lost surface area, complexity, and perimeter, indicating age-related declines in ATP synthesis and interaction capacity. Concomitantly, muscle area, exercise capacity, and mitochondrial dynamic proteins showed age-related losses. Exercise stimulation restored mitofusin 2 (MFN2), which we show is required for mitochondrial structure. Furthermore, we show that this pathway is evolutionarily conserved with Marf, the MFN2 ortholog in *Drosophila*, as Marf knockdown alters mitochondrial morphology and leads to the downregulation of genes regulating mitochondrial processes. Our results define age-related structural changes in mitochondria and further suggest that exercise may mitigate age-related structural decline through modulation of mitofusins.

Introduction:

Aging is an inescapable biological process that is characterized by a progressive decline in physiological and metabolic functions. During the aging process, changes in metabolic homeostasis, muscle mass, and function have been observed across species and sexes (Greenlund & Nair 2003; Tay et al. 2015). Although pluralistic effects of aging exist that contribute to increasing vulnerability to disease, in skeletal muscle, sarcopenia, which consists of muscle degeneration and progressive loss of muscle mass, remains a global health issue (Martinez et al. 2015; Greenlund & Nair 2003). Although the prevalence of sarcopenia remains poorly elucidated, past cross-sectional analyses have shown that approximately 20% of hospitalized adult patients meet the criteria for sarcopenia, with risk factors including old age and obesity (Sousa et al. 2015). Currently, sarcopenia accounts for approximately 1.5% of healthcare expenditures in the United States, and as the population worldwide increasingly ages, the burden of sarcopenia will only be exacerbated (Coen et al. 2019; Filippin et al. 2015). Generally, sarcopenia occurs at approximately 40 years of age with a loss of 8% of muscle mass per decade; then, the rate increases to 15% of muscle mass loss per decade after 70 years (Kim & Choi 2013). Sarcopenia, in turn, increases the risk of mortality and disability because of an increased risk of adverse events including falls, fractures, and functional decline, cumulatively resulting in a decreased quality of life (Filippin et al. 2015).

Although sarcopenia has increasingly been studied to reduce its burden on healthcare systems globally, therapies have been limited. Because the mechanism of sarcopenia remains poorly understood (Greenlund & Nair 2003), no clinical treatment, other than nutritional changes and a regular exercise regimen, exists to mitigate its development (Phu et al. 2015; Taaffe 2020). However, the underlying molecular mechanisms driving these age-related changes and the reason why exercise may be able to reverse them remain insufficiently understood. Recently, mitochondria have increasingly arisen as a potential target to mitigate sarcopenia because mitochondrial functional changes often precede the loss of muscle mass and function characteristic of sarcopenia (Campo et al. 2018; Coen et al. 2019; Hepple 2014). In *Caenorhabditis elegans*, mitochondrial content correlates strongly with lifespan, with mitochondrial network structure declines arising antecedent to sarcomere loss (Gaffney et al. 2018). We have previously shown in a murine model that mitochondrial structure in skeletal muscle undergoes reductions in size and changes in morphology during aging, which may confer reduced functional capacity antecedent to the development of sarcopenia (Vue, Garza-Lopez, et al. 2023). However, mitochondrial structure in human skeletal muscle during aging remains poorly defined, especially in relation to exercise.

Although mitochondria are generally characterized by their role in ATP synthesis, their pluralistic roles extend far beyond this, including metabolic signaling and calcium homeostasis, cumulatively linking mitochondria to the aging process (Bratic & Larsson 2013; Campo et al. 2018). These organelles are not static but highly dynamic, undergoing constant cycles of fission, mediated by effectors such as dynamin-related protein 1 (DRP1), and fusion, mediated by effectors such as optic atrophy protein 1 (OPA1) and mitofusins 1 and 2 (MFN1 and MFN2), to adapt to the cellular environment (Dong et al. 2022; Chan 2012). Interruptions of either of these processes can interfere with mitochondrial function, cause dysfunction, and be representative of pathology (Chan 2012; Bartsakoulia et al. 2018; Chen et al. 2005). Recently, an age-associated loss of OPA1 was linked to reduced skeletal muscle mass (Tezze et al. 2017). Beyond fusion and

fission dynamics, these same regulators may often give rise to alterations in the mitochondrial network and morphology (Chen et al. 2005; Liu & Hajnóczky 2011). Thus, it is increasingly understood that mitochondria change their three-dimensional (3D) morphology to unique phenotypes that are representative of their cellular state, such as during stress (Glancy et al. 2020). For example, donut-shaped mitochondria may emerge as a pathology-induced mechanism to increase surface area at the expense of volume (Hara et al. 2014). Decreased volume means less space for the folds of the inner mitochondrial membrane, known as cristae, which optimize ATP synthesis (Cogliati et al. 2016). However, the increased surface area may also allow for increases in mitochondrial–endoplasmic reticulum contact sites (MERCs), which may function in alternative biochemical roles such as in calcium homeostasis (Bustos et al. 2017). In tandem, mitochondrial dynamics can result in unique 3D structures that may play pivotal roles in the aging process and the associated muscle degeneration.

Previously, we performed 3D reconstruction for the volumetric rendering of mitochondria using manual contour tracing, which provides information on mitochondrial phenotypes, including those in murine skeletal muscle during aging (Vue, Garza-Lopez, et al. 2023). This method is facilitated by serial block-face scanning electron microscopy (SBF-SEM), which given its large range, allows for large-volume renderings and mitochondrial networks to be accurately replotted (Marshall, Neikirk, et al. 2023; Courson et al. 2021). Previously, the 3D structure of human skeletal muscle was examined in the context of mitochondrial DNA (mtDNA) diseases (Vincent et al. 2019). Traditional 2D techniques examining aged skeletal muscle cells of humans have shown large mitochondria with disrupted cristae (Beregi et al. 1988). However, mitochondria in aged human skeletal muscle tissue were observed to shrink in a sex-dependent manner (Callahan et al. 2014), and aged mouse skeletal muscle tissue has been found to have increased branching during aging due to an increased MFN2-DRP1 ratio (Leduc-Gaudet et al. 2015). These conflicting results limit our understanding of mitochondrial ultrastructure in sarcopenia. Importantly, to our knowledge, the 3D structure of human skeletal muscle mitochondria during the aging process has yet to be defined.

In this study, we employ a multi-pronged approach to explicate the interplay among aging, mitochondrial dynamics, and exercise therapies. Utilizing both human and murine models, as well as the genetically tractable model organism *Drosophila melanogaster*, we offer an analysis of how aging affects skeletal muscle mass and mitochondrial 3D architecture. We further investigate whether these age-related changes are evolutionarily conserved and explore the potential for exercise to mitigate these detrimental effects. Our findings offer insights into the role of mitochondrial structural changes in age-associated muscle degeneration and metabolic shifts and elucidate potential mechanisms for exercise as a modulatory tool for age-related deficiencies. We further highlight hematological changes that occur in the aging process and show that mitochondrial structural rearrangement is mechanistically likely responsible for the mitigation of sarcopenia by exercise. Our findings highlight MFN2 as a potential therapy for sarcopenia and an effector that mediates exercise-dependent impairment of sarcopenia development.

Methods:

Human Sample Cohort:

Several different human cohorts across multiple countries were utilized for this study. Specimens for all 3D reconstructions (Figures 2–3) were collected at Vanderbilt University Medical Center. Collection of human quadriceps tissue was approved by the Vanderbilt University Institutional Review Board (IRB) under the title "Mitochondria in Aging and Disease -- study of archived and autopsy tissue" with an associated IRB number of 231584. All other human samples were obtained from Brazilian cohorts according to the CAEE (Ethics Appreciation Presentation Certificate) guidelines. Samples from young individuals were collected, and experiments were performed under CAAE number 61743916.9.0000.5281; samples from older individuals were collected under CAAE number 10429819.6.0000.5285. Mixtures of male and female samples (specified in figures) were used in all studies, with a general cutoff age of 50 years for humans.

Magnetic Resonance Imaging Data:

Full sample characteristics are available in Supplemental File 1.

Segmentation and Quantification of 3D SBF-SEM Images Using Amira: The protocols followed previously established methods (Vue, Neikirk, et al. 2023; Crabtree et al. 2023; Garza-Lopez et al. 2022; Vue, Garza-Lopez, et al. 2023). Briefly, after isolated human quadriceps were excised and cut into 1 mm^3 samples, they were fixed in 2% glutaraldehyde in 0.1 M cacodylate buffer and processed using a heavy metal protocol adapted from a previously published protocol (Courson et al. 2021; Mustafi et al. 2014). Following immersion in 3% potassium ferrocyanide and 2% osmium tetroxide for 1 hour at 4°C, the tissue was filtered in 0.1% thiocarbohydrazide for 20 min and 2% osmium tetroxide for 30 min, and de-ionized H_2O washes performed between each step. Tissues were incubated overnight in 1% uranyl acetate at 4°C. Next, the samples were immersed in a 0.6% lead aspartate solution for 30 min at 60°C and then dehydrated in graded acetone dilutions. The samples were embedded in fresh Epoxy TAAB 812 hard resin (Aldermaston, Berks, UK) and polymerized at 60°C for 36–48 hours. The block was sectioned for transmission electron microscopy (TEM) to identify the area of interest, trimmed to a 0.5 mm × 0.5 mm region of interest (ROI), and glued to an aluminum pin. Finally, the pin was placed into an FEI/Thermo Scientific Volumescope 2 scanning electron microscopeimaging.

Following fixation of the samples, 3D reconstruction of SBF-SEM orthoslices was performed using previously published techniques (Garza-Lopez et al. 2022; Hinton et al. 2023; Neikirk et al. 2023; Vue, Garza-Lopez, et al. 2023; Vue, Neikirk, et al. 2023; Crabtree et al. 2023). Briefly, using contour tracing in Amira to perform 3D reconstruction, 300−400 orthoslices and 50–100 serial sections were stacked, aligned, and visualized. An individual blinded to the experimental conditions who was familiar with organelle morphology manually segmented the structural features on sequential slices of micrograph blocks.

Murine-derived Myotubes:

As previously described (Pereira et al. 2017), satellite cells were isolated from C57Bl/6J mice, and cells were derived and plated on BD Matrigel-coated dishes. Following our previously published protocol (Stephens et al. 2023), cells were activated to differentiate into myoblasts and myotubes.

To separate myoblasts, after reaching 90% confluence, myoblasts were differentiated to myotubes in DMEM/F-12 containing 2% fetal bovine serum (FBS) and 1× insulin-transferrin-selenium. Three days after differentiation, myotubes were infected to deliver 1 µg of CRISPR/Cas9 plasmid (Santa Cruz CRISPR Plasmid) to delete *MFN1*, *MFN2*, or both (double knockout, DKO), which was validated by quantitative PCR (qPCR). Experiments were performed 3–7 days after infection.

Cell Culture:

After isolation, human and primary mouse myotubes were maintained in a mixture of DMEM/F-12 (Gibco: Waltham, MA, USA) containing 20% FBS (Gibco), 10 ng/ml basic fibroblast growth factor, 1% penicillin/streptomycin, 300 µl/100 ml Fungizone, 1% non-essential amino acids, and 1 mM β-mercaptoethanol. On alternate days, the medium was replaced after cells were washed with phosphate-buffered saline (PBS) to ensure all excess media is removed.

RNA Extraction and Real-Time qPCR:

Using a RNeasy kit (Qiagen Inc.), RNA was isolated and subsequently quantified through absorbance measurements at 260 nm and 280 nm using a NanoDrop 1000 spectrophotometer (NanoDrop products, Wilmington, DE, USA). Using a High Capacity cDNA Reverse Transcription Kit (Applied Biosciences, Carlsbad CA), isolated RNA (~1 µg) was reverse transcribed and then amplified by real-time qPCR with SYBR Green (Life Technologies, Carlsbad, CA), as previously described (Boudina et al. 2007). For each experimental condition, triplicate samples (~50 ng DNA each) were placed in a 384-well plate before undergoing thermal cycling in an ABI Prism 7900HT instrument (Applied Biosystems). The thermal cycling conditions were set as follows:

Cycle Count	Temperature	Time
1	95°C	10 min
40	95°C	15 s
	59°C	15 s
	72°C	30 s
1	95°C	15 s
1	60°C	15 s
1	95°C	15 s

The final results are normalized to those of glyceraldehyde-3-phosphate dehydrogenase and are presented as relative mRNA fold changes.

In Vitro Exercise Stimulation:

In vitro exercise simulation using electric pulse stimulation was performed as previously described **(Evers-van Gogh et al. 2015; Lambernd et al. 2012)**. Briefly, following human or skeletal myotube differentiation or with C2C12 cells, the cells were starved by culturing in DMEM without FBS. The medium was replaced directly prior to stimulation. Electrical stimulation was administered through carbon electrodes using a C-Pace 100 pulse generator (IonOptix, Milton, MA, USA) in a C-dish. The stimulation parameters were set at a frequency of 1 Hz, a pulse duration of 2 ms, and an intensity of 11.5 V, with treatment sustained for 4.5 or 24 hours. Conditioned medium was harvested from both stimulated and non-stimulated conditions and then centrifuged at 800 rpm for 5 min, and the samples were stored at −80°C. A mixture of growth medium DMEM/F-12 containing 10% FBS and conditioned medium containing 0% FBS in equal parts was prepared and applied to specified cell lines. Western blotting or qPCR was then performed as described.

Western Blotting:

As previously described (Hinton et al. 2022), to obtain protein extracts from differentiated myotubes and C2C12 cells, we washed cells with ice-cold PBS and then added cold lysis buffer [25 mM Tris HCl, pH 7.9, 5 mM $MgCl_2$, 10% glycerol, 100 mM KCl, 1% NP40, 0.3 mM dithiothreitol, 5 mM sodium pyrophosphate, 1 mM sodium orthovanadate, 50 mM sodium fluoride, and protease inhibitor cocktail (Roche Applied Science, Penzberg, Germany)]. Following scraping of the cells, a 25-gauge needle was used to homogenize the cells before they were centrifuged at 14,000 rpm for 10 min at 4°C. Following centrifugation, the supernatants were collected and diluted with Laemmli sample buffer to obtain a final concentration of 1×. We performed sodium dodecyl sulfate-polyacrylamide gel electrophoresis with 1× concentrated cell lysates, and proteins were transferred to nitrocellulose membranes (BioRad, Berkeley, California, USA). Blocking of membranes was performed with 5% bovine serum albumin in Tris-buffered saline with Tween-20. Primary antibodies used for western blotting and their working dilutions included fibroblast growth factor 21 (FGF21) and calreticulin (CALR). Following incubation of three biological replicates for each protein of interest, quantification was performed using Image Studio Lite Ver 5.2.

TEM Analysis

As previously described (Hinton et al. 2023), cells were fixed in 2.5% glutaraldehyde diluted in sodium cacodylate buffer for 1 hour at 37°C and then embedded in 2% agarose, postfixed in buffered 1% osmium tetroxide, stained with 2% uranyl acetate, and dehydrated with a graded ethanol series. Following EMbed-812 resin embedding, 80-nm sections were cut on an ultramicrotome and stained with 2% uranyl acetate and lead citrate. Images were acquired on a JEOL JEM-1230 transmission electron microscope operating at 120 kV.

NIH ImageJ software (Schneider et al. 2012) was used to manually trace and analyze all mitochondria or cristae using the freehand tool (Parra et al. 2013). Measurements of mitochondrial area, circularity, and number were performed using the Multi-Measure ROI tool in ImageJ (Lam et al. 2021; Neikirk et al. 2023; Parra et al. 2013). We used three distinct ROIs, all of the same magnification, in ImageJ to examine cristae morphology and determine their area and number. The sum of the total cristae area divided by the total mitochondrial area was used as a proxy to determine cristae volume (Patra et al. 2016).

Drosophila Strains and Genetics

Flies were cultured on standard yeast-cornmeal agar medium in vials or bottles at 25°C with a 12h12h12-hour light/dark cycle. The Mef2-Gal4 (also known as P{GAL4-Mef2.R}3) driver line was used to direct the expression of upstream activating sequence (UAS) transgenes, specifically in skeletal muscle. UAS-mitoGFP (II) was used to visualize mitochondria. RNAi knockdown (KD) lines originating from transgenic RNAi lines were obtained from the Bloomington Drosophila Stock Center and included *UAS-Chchd3 RNAi* (51157), UAS-Mitofilin RNAi (63994), *UAS-QIL1 RNAi* (44634), *UAS-Drp1 RNAi* (51483), *UAS-Marf RNAi* (55189), and *UAS-Opa1-like RNAi* (32358). Chromosome designations and additional strain details are available on FlyBase (http://flybase.org). Male and female flies were analyzed together, as no sex differences in mitochondrial morphology were observed in wild-type muscle. The Mef2-Gal4 strain served as a control within the respective genetic backgrounds.

Mitochondrial Staining

Thoraces from 2–3-day-old adult *Drosophila* were dissected in 4% paraformaldehyde (PF, Sigma))), and indirect flight muscles were isolated as described previously by Katti et al., 2022{Katti, 2022 #462}. Isolated muscles were fixed in 4% PF for 1.5 hours with agitation, followed by three 15-min washes with PBSTx (phosphate-buffered saline + 0.3% Triton X-100). Mitochondria were visualized by staining with either 200 nM for MitoTracker™ Red FM (M22425, ThermoFisher) for 30 min or by mitochondrial-targeted green fluorescent protein (GFP) expressed from UAS-mito-GFP under the control of Mef2-Gal4. F-actin was stained by incubating muscles in 2.5 μg/ml phalloidin-TRITC (Sigma) in PBS for 40 min at 25°C. Stained muscles were mounted in Prolong Glass Antifade Mountant with NucBlue (ThermoFisher) and imaged using a Zeiss LSM 780 confocal microscope.

Mitochondrial Quantification

Mitochondria were quantified by imaging muscle fibers using fluorescence microscopy. MitoTracker Green FM dye (Invitrogen) or mito-GFP, as mentioned above, were used to label mitochondria. Images were acquired at 60x60x60× magnification and were analyzed using ImageJ software. Images were divided into regions, and mitochondria spanning three sarcomeres (from the Z-disc of the first sarcomere to the Z-disc of the fourth sarcomere) were selected for analysis. The number of mitochondria in three sarcomeres was manually counted using ImageJ.

Mitochondrial Area and Circularity Analysis

Mitochondrial morphology was assessed by quantifying mitochondrial circularity and area, which were measured using ImageJ software. The mitochondrial area was measured for every mitochondrion in the region. Circularity is a measure of how closely a shape approximates a perfect circle, calculated as $4\pi \times (\text{area}/\text{perimeter}^2)$. A value of 1.0 indicates a perfect circle. Increased mitochondrial circularity indicates a shift toward more rounded mitochondria and loss of elongated mitochondrial networks. Graphs were created and statistical analysis was performed using GraphPad Prism (version 9.0, La Jolla, CA, USA).

RNA Sequencing

Using the same method of mRNA isolation as described above, for RNA sequencing, a list differentially expressed genes (DEGs) was compiled from RNA-sequencing results ($p_{adj}<0.05$

and absolute log_2 fold change>0.66) and were analyzed for potential enriched pathways using Ingenuity Pathway Analysis (IPA, QIAGEN) and Gene Set Enrichment Analysis (GSEA) with WebGestalt (www.webgestalt.org) **(Liao et al. 2019)**. For IPA analysis, enriched pathways were considered significant when applying an absolute activation Z-score of >2 and p_{adj}<0.05. For GSEA results, an absolute enrichment score of >2 and p_{adj}<0.05 was considered significant.

Data Analysis

Black bars in graphs represent the standard error, and dots represent individual data points. All analyses were performed using the GraphPad Prism software package, with specific tests indicated in the figure legends. A minimum threshold of $p < 0.05$ indicated a significant difference. Higher degrees of statistical significance (**, ***, ****) are defined as $p < 0.01$, $p < 0.001$, and $p < 0.0001$, respectively.

Results:

Human Aging Causes Alterations in Muscle Size

Previous studies have utilized magnetic resonance imaging of thigh cross-sectional area (CSA) as a proxy to determine muscle size (Beneke et al. 1991). Furthermore, the muscle and bone relationship has been examined to investigate sarcopenia because the intra-individual muscle mass loss during aging can be determined (Maden-Wilkinson et al. 2014). Thus, we initially utilized magnetic resonance imaging to determine how the skeletal muscle structure in the thigh and femur is remodeled during the aging process. By enrolling female and male participants (Figure 1A–D), we created a "young" cohort consisting of individuals from 18 to 50 years old and an "old" cohort of individuals older than 50 years old (Supplemental File 1). When male and female subjects were combined, thigh or femur CSA was not significantly differentiated across the aging process (Supplemental Figure 1A). However, we observed slight sex-dependent differences during the aging process (Supplemental Figures 1B–C). Males had significantly decreased thigh CSA (Figure 1E–E'), while females had increased femur CSA (Figure 1F–F'). For both sexes, however, the muscle area relative to the bone area in the thigh region generally decreased (Figure 1G–G'). These age-related losses in muscle mass validated the occurrence of muscle atrophy in the human quadriceps. While we could not confirm subjects had sarcopenia, these results support the observation of an age-related decline in muscle mass. Next, we sought to explicate whether these age-related losses in muscle mass are correlative with alterations in 3D mitochondrial structure.

Aging is Associated with Changes in Human Skeletal Muscle Mitochondrial Structure and Dynamics

Based on the age-related loss of thigh CSA, we sought to understand how the aging process may lead to this degeneration of muscle mass. Because mitochondrial size and morphology are dynamic, responding to environmental stimuli and conferring changes in the metabolic effects of mitochondria such as respiratory efficiency (Frey & Mannella 2000; Glancy et al. 2020), we first sought to determine whether mitochondrial dynamics and morphology are altered as a result of the aging process. Utilizing qPCR, we surveyed pertinent mitochondrial proteins from skeletal muscle samples of 18–40-year-old (young) and 60–90-year-old (old)

humans. In human skeletal muscle genes associated with mitochondrial fusion and fission dynamics (Figure 2A–D), the mitochondrial contact site and cristae organizing system (MICOS) complex (Figure 2E–G) and MERCs (Figure 2H–J) were altered with aging. Specifically, fusion (Mfn1, Mfn2, and Opa1; Figure 2A–C) and fission (Drp1; Figure 2D) proteins along with the MICOS complex (Mic19, Mic25, and Mic60; Figure 2E–G) were decreased with aging. Reductions in fusion and fission proteins were validated by previous studies that showed age-related losses of mitochondrial dynamic proteins in human skeletal muscle (Seo et al. 2010; Crane et al. 2010). Additionally, we previously showed that age-related loss of the MICOS complex results in reductions in mitochondrial volume in murine skeletal muscle (Vue, Garza-Lopez, et al. 2023). Interestingly, however, MERC proteins (Grp75; Ip3r3, and Vdac3; Figure 2H–J) were upregulated in human skeletal muscle during aging. These results are suggestive of decreases in cristae integrity, mitochondrial dynamics, and mitochondrial structural integrity; however, the exact 3D structural remodeling of mitochondria in human skeletal muscle remains unclear. Therefore, we sought to understand how these changes in mRNA transcripts manifested as alterations in mitochondrial structure.

We utilized SBF-SEM to perform 3D reconstruction of mitochondria (Figure 2K). SBF-SEM has a lower resolution than conventional TEM imaging (Marshall, Neikirk, et al. 2023), but its high range offers advantages over other 3D light-based imaging methods (Marshall, Damo, et al. 2023; Marshall, Krystofiak, et al. 2023). We collected quadriceps samples from young (under 50 years old) and old (over 50 years old) individuals. We utilized a mix of human quadriceps from both males and females because previous studies have generally shown that sarcopenia occurs at a similar rate in both sexes (Tay et al. 2015). According to previous methods (Vue, Garza-Lopez, et al. 2023), 50 z-directional SBF-SEM micrographs, also known as “orthoslices”, were obtained (Figure 2L–L’), and the 3D structure of intermyofibrillar mitochondria, or mitochondria between fibrils (Vendelin et al. 2005), was rendered through manual contour segmentation (Figure 2M–M’). This time-consuming manual process allowed for mitochondria structure to be verified and for observation of the complete mitochondrial 3D structure in young and old human skeletal muscle (Figure 2N–N’). Three ROIs were considered in each experimental condition, within which approximately 250 mitochondria were quantified for a total of 750 mitochondria (Supplemental Figure 2). Once rendered, we found no significant change in mitochondrial volume across the aging process (Figure 2K); however, both the mitochondrial surface area and perimeter showed age-dependent decreases (Figure 2P–Q). While mitochondrial volume can be indicative of the total capacity for energy production (Gallo et al. 1982), it can also be indicative of mitochondrial swelling, an event that typically occurs antecedent to apoptosis (Safiulina et al. 2006). Thus, to better understand how mitochondrial structure undergoes age-related changes, we examined its complexity.

<u>Aging Causes Human Skeletal Muscle Mitochondria to Become Less Complex</u>

Previously, mitochondrial complexity has been shown to be altered with mtDNA defects in human skeletal muscle (Vincent et al. 2019), yet how the 3D complexity changes with aging remains unclear. Based on structural changes in surface area, we sought to determine whether aging conferred a modulatory effect on mitochondrial complexity. Using the same samples as before, quadriceps intermyofibrillar mitochondria from young and old human subjects were viewed from transverse (Figure 3A–B) and longitudinal points of view (Figure 3A’–B’). Based

on the views of mitochondria from these disparate axes, we observed that mitochondria from young individuals generally appeared more elongated, while those from older individuals appeared more compact. To confirm this finding, we examined mitochondrial sphericity, which showed age-related increases, in which mitochondria generally appeared to have a rounder shape (Figure 3C). As a secondary 3D form-factor measurement, we employed a mitochondrial complexity index (MCI), which represents the ratio of the surface area and volume (Vue, Garza-Lopez, et al. 2023; Vincent et al. 2019). While analogous to sphericity, the MCI is important to measure as it offers insight into shape mostly independent of volume, principally taking into account factors such as increases in branches and surface area (Vincent et al. 2019). The MCI indicated reduced complexity in samples from older individuals (Figure 3D). To further visualize how these reductions in complexity arise, we used Mito-otyping, a method of mitochondrial organization based on their relative volume, to visualize changes in the complexity (Vincent et al. 2019). Mito-otyping showed that, in young individuals, mitochondria were more complex and showed diverse phenotypes, while older individuals had mostly compact and spherical mitochondria, indicating that the surface area to volume ratio decreases during the aging process (Figure 3E). While slight intra-cohort variability in the MCI was observed (Supplemental Figure 2E), the relatively low intra-individual variability indicated that changes in mitochondrial complexity and morphology were generally ubiquitous across the mitochondria surveyed. Together, these results indicate that although mitochondrial volume is not reduced in aged human quadriceps, the mitochondrial morphology undergoes significant alterations, which may be representative of mitochondrial dysfunction and associated sarcopenia.

Aging Modulates Exercise Ability, Immune and Glucose Responses

Next, we sought to understand the functional implications of these age-related changes. Because no pharmacological interventions for sarcopenia yet exist, exercise has remained a principal therapeutic approach to mitigate this condition (Phu et al. 2015). Inversely, however, the muscle mass loss caused by sarcopenia can reduce endurance and strength, which suggests that adequate exercise prior to aging may be necessary (Greenlund & Nair 2003). We sought to better understand how individuals, with potential sarcopenia, may have impaired strength and endurance. We included a new cohort of individuals constituting both males and females, divided them into “young” (under 35 years old) or “old” (over 60 years old) categories, and subjected them to various exercises (Supplemental File 2). We observed that decreases in exercise strength and endurance occurred during aging with slight sex-dependent differences (Supplemental Figure 3). Specifically, in both females and males, we showed that generally, weight and body mass index remained unchanged or minimally changed when comparing young and old individuals, indicating that changes in strength are not primarily attributable to changes in overall mass (Figure 4A–B’). Both males and females also had significant decreases in walking distance and the associated maximum amount of oxygen utilized during intense exercise (VO_2) suggesting decreased aerobic capacity (Figure 4C–D). Notably, this difference was slightly more pronounced in females than in males (Figure 4C’–D’). When examining strength, we showed that the grip strength of both arms decreased, indicating decreased muscle mass (Figure 4E–F’). Interestingly, while young males had greater grip strength than females, males also exhibited a more significant decrease with aging, resulting in aged males and females having similar grip strength (Supplemental Figure 3F–G). To further explore how muscle endurance changes, we examined both upper and lower body endurance, which showed much more drastic decreases in

lower body endurance, with slight sex-dependent differences (Figure 4G–H'). Together, these results indicate that with aging, both males and females lose endurance and muscle strength, indicative of sarcopenia occurring along with the 3D structural mitochondrial remodeling that we observed.

To further understand potential mechanisms underpinning age-related changes, we determined whether any factors in blood or plasma exhibited alterations. We found that aging had numerous effects on blood serum molecules (Supplemental Figure 4). Of these, changes in glucose metabolism, hemoglobin-carrying capacity, and immune responses were notable (Figure 4I–N). Glycated hemoglobin levels, which increased with aging (Figure 4I), are used to gauge average blood glucose over approximately the previous 3 months and serve as a better index for long-term glycemic exposure than fasting or blood glucose levels (Zhang et al. 2010). Similarly, in the older cohort, the mean glucose concentration was significantly increased, suggesting impaired glucose homeostasis with age (Figure 4J). When investigating the mean corpuscular hemoglobin, which signifies the average amount of hemoglobin in red blood cells, we noticed a significant increase in older individuals (Figure 4K). This finding is suggestive of increased oxygen-carrying capacity, which can affect muscle endurance and function and may be a response to altered mitochondrial respiration (Xuefei et al. 2021). While alterations in hemoglobin can affect mitochondria through oxidative stress generation (Pandya et al. 2021), hemoglobin serves multifaceted functions, and peripheral blood mononuclear cells can also increase intracellular hemoglobin (Brunyanszki et al. 2015). Thus, we next investigated how aging increases the immune response. As expected, because autoantibody responses generally increase in the elderly population (Yung 2000), we found that although erythrocytes were decreased, monocytes and band cells were both increased in the aged group compared with those in the young group. Notably, an elevated band cell count suggests an active inflammatory or infectious process (Mare et al. 2015). Together, these findings show that glucose levels increase concomitantly with immune responses during the human aging process.

Next, we sought to determine whether exercise, which has extensively been described as an effective therapy for sarcopenia (Phu et al. 2015; Taaffe 2020), mechanistically acts to modulate these age-dependent alterations in immune signaling and glucose metabolism. To explore this mechanism, we used a previously validated method of electric pulse stimulation, which simulates exercise *in vitro* (Evers-van Gogh et al. 2015). We found that with *in vitro* electrical stimulation for 4.5 hours, L-lactate and glucose levels both increased in human myotubes (Figure 4O–P), validating that cells exhibit an "exercised" phenotype. Specifically, lactate can serve as a valuable energy source, but its accumulation can also be linked to muscle fatigue (Nalbandian & Takeda 2016). Increased glucose levels reflect the body's reliance on carbohydrates for energy during exercise (Mul et al. 2015). We further recapitulated these findings with 24 hours of electrical stimulation, which showed no significant differences and suggested that 4.5 hours is sufficient to create an exercised phenotype (Figure 4Q–R). Once we validated this method of *in vitro* exercise, we examined three cell types: C2C12 cells, primary myotubes, and human myotubes. In all three cell types, interleukin 6 (IL6; representative of the immune and inflammatory response) and FGF21 (representative of glucose metabolism) both increased with exercise (Figure 4S–X). Notably, this increase in IL6 is consistent with previous studies (Beavers et al. 2010), suggesting an acute response that may not be chronic. However, this increase does not suggest that exercise mitigates sarcopenia through reductions in the immune response. Notably, however, FGF21 is well understood to be antihyperglycemic, with increases in circulating FGF21 levels occurring concomitantly with improved glucose tolerance

and decreased blood glucose (Xu et al. 2009). Beyond broad associations of mitochondrial dysfunction with insulin sensitivity, FGF21 has previously been implicated in interactions with mitochondrial dynamic proteins (Pereira et al. 2017; Pereira et al. 2021).

Together, these findings demonstrate that exercise has a modulatory effect on age-related changes in glucose homeostasis, indicating that aging effects can be modulated in part through exercise. Notably, this finding is suggestive that exercise mitigates sarcopenia in FGF21-dependent pathways, which may involve mitochondrial dynamic alterations. Thus, we turned our attention to understanding whether mitochondrial structure can be modulated by exercise.

Exercise Restores Age-related Loss of Mitofusin 2

As previously shown, exercise may be an important mechanism by which mitochondrial quality is protected as healthy aging, including the mitigation of sarcopenia, occurs (Cartee et al. 2016). Past seminal findings have shown that MFN2 plays a critical role in muscular aging and associated mitochondrial dysfunction through age-dependent loss of MFN2 and concomitant inhibition of mitophagy (Sebastián et al. 2012). We sought to extend these findings to determine whether MFN2 further plays a critical role in mitochondrial structure remodeling in exercise to protect against sarcopenia. Validating previous findings, we found that loss of MFN2 occurs in various murine tissue types during aging (Figure 5A–D), which parallels the loss we observed previously in human skeletal muscle (Figure 2B). Thus, we aimed to determine whether exercise can rescue these levels (Figure 5E–E’), which would suggest a reversal of age-related deficits in mitochondrial dynamics and structure. Again, subjecting both C2C12 (Figure 5F–I) and primary murine-derived myotubes (Figure 5F’–I’) to *in vitro* electric stimulation, we verified the ability of our *in vitro* method to induce a prolonged exercise phenotype. We observed an increase in L-lactate levels and a decrease in glucose levels following 4.5 or 24 hours of exercise (Figures 5F–I’), which may reflect a metabolic state associated with high-intensity or prolonged exercise. Specifically, this finding suggests a shift toward anaerobic metabolism, muscle fatigue due to acidosis, and the utilization of glucose and glycogen for energy (Goodwin et al. 2007). Western blotting (Figure 5E–E’) also indicated thatMFN2 and CALR levels are increased in both C2C12 and primary myotubes (Figure 5J–K’), indicating that mitochondrial and MERC dynamics are increased following exercise. MFN2 and CALR are interestingly both MERC proteins (Han et al. 2021; Peggion et al. 2021), but MFN2 also plays a pluralistic role in mitochondrial fusion.

Because we noted that exercise may reverse age-related loss of MFN2, we sought to better elucidate the role of MFN2 in mitochondrial structure. While past studies have consistently shown that MFN2 deficiency is associated with increased MERC tethering (Leal et al. 2016; De Brito & Scorrano 2008), some studies have shown that MFN2 modulation does not necessarily impact mitochondrial structure alone (Cosson et al. 2012). In some species, such as *Drosophila melanogaster*, a single protein is functionally analogous to both MFN1 and MFN2 (Dorn et al. 2011; Katti et al. 2021). Thus, to better understand the structural impacts of age-related mitofusin loss, we knocked out both MFN1 and MFN2 individually as well as contiguously (DKO) and utilized TEM analysis (Lam et al. 2021) to consider ultrastructural changes in mitochondria and cristae in murine-derived myotubes (Figures 5L–S). MFN1 knockout (KO) and DKO resulted in increased mitochondrial numbers and decreased average area (Figure 5T–U). Similarly, MFN2 KO reduced mitochondrial area but inversely increased mitochondrial number, resulting in no significant change in mitochondrial count, which trended downwards (Figure 5T–U). Notably, all conditions caused the circularity index to increase

(Figure 5V), resulting in more regularly shaped small mitochondria, suggestive of reduced fusion. Loss of fusion proteins may also affect cristae ultrastructure (Vue, Neikirk, et al. 2023); therefore, we specifically investigated MFN2 and the DKO condition as regulators of cristae morphology. MFN2 KO resulted in reductions in cristae number, volume, and surface area, suggesting a reduced oxidative capacity (Figure 5W–Y). The same effects on mitochondrial and cristae morphology were observed in the DKO condition, marked by smaller, more plentiful mitochondria with reductions in cristae count and volume (Figure 5W–Y).

These structural changes confirmed prior studies indicating that the loss of MFN1 and MFN2 results in structural alterations with redundant yet distinct roles (Chen et al. 2003). The results also validated previous literature showing that age-related losses of MFN1 and MFN2, along with other proteins associated with biogenesis, are reversed by exercise training (Koltai et al. 2012). Furthermore, the age-related loss of both MFN1 and MFN2 (Figures 2A–B) suggests that structural rearrangements in mitochondria may arise due to loss of MFN1 and MFN2. Additionally, exercise may be able to ameliorate some of the age-related structural losses in mitochondria through increasing MFN2 (Figures 5J–J'). However, to better understand the functional impacts of mitofusins and whether the structural rearrangements caused by mitofusins are evolutionarily conserved, we examined a *Drosophila* model.

Mitofusins are Functionally Required for Mitochondrial Regulation and Structure

We focused on flight skeletal muscle in the *Drosophila* model (Figure 6A). We knocked down Mitochondrial Assembly Regulatory Factor (MARF KD), which is functionally analogous to MFN1 and MFN2, and verified that the gene was silenced at the mRNA transcript level (Figure 6B). Then, we showed that the loss of MARF altered overall development (Figure 6C), motor skills (Videos 1–4), and fly steps, or walking motion, (Figure 6D) in *Drosophila*. Furthermore, RNA sequencing was performed in MARF KD muscle that revealed widespread transcriptional changes including Marf (Figure 6E). Pathway analysis for contributing canonical pathways using IPA indicates a primary defect in mitochondrial and metabolic-related pathways including oxidative phosphorylation, the TCA cycle, glycolysis, and gluconeogenesis (Figures 6F; Supplemental File 3). These findings provide a link between mitochondrial structural changes observed with aging and the metabolic basis of age-related diseases. Additional pathway analyses support the notion that MARF KD leads to mitochondrial dysfunction, metabolic defects, and abnormal reactive oxygen species production while also inhibiting cell division processes (Supplemental Figure 5; Supplemental File 4). RNA sequencing also revealed that mitochondrial biogenesis and its upstream transcriptional regulators (e.g., PPARGC1A, Esrra) are generally inhibited by MARF KD and correlate with changes in mitophagy, sphingolipids, mammalian target of rapamycin (mTOR) and DNA synthesis (Figure 6 G, Supplemental Figure 6).

Based on these pathway and functional changes, we aimed to understand the changes in mitochondrial dynamics caused by loss of MARF. We first examined the mRNA levels of several key mitochondrial proteins following MARF silencing. As expected, MARF KD decreased mRNA transcripts of MARF (Figure 6H), with slight variation from validation in Figure 6B. Interestingly, however, OPA1 and DRP1 were both increased (Figures 6I–J), indicating the upregulation of dynamic proteins without a clear preference toward fusion or fission. We also noticed that endoplasmic reticulum (ER) stress is increased with upregulation of ATF4, ATF6, and IRE1 (Figures 6K–M), which was validated by previous studies showing that MFN2

deficiency causes ER stress (Ngoh et al. 2012). Notably, ER stress can result in MERC formation (Wan et al. 2014). Therefore, we further examined MERC proteins along with GRP75 and VDAC3, which were increased and decreased, respectively, with loss of MARF (Figures 6N–O). Together, these findings suggested multiple changes in dynamics with unclear implications, thus we sought to understand specific structural changes using TEM. When MARF was knocked out (Figures 6P–S), the mitochondrial number did not change (Figure 6T), which may be because of increases in both DRP1 and OPA1, resulting in increased fusion and fission. Additionally, paralleling the results of DKO condition in myotubes, MARF KD resulted in smaller mitochondria with greater circularity (Figures 6U–V). Significant decreases in cristae volume and surface area were observed, indicating large impairments in mitochondrial oxidative phosphorylation (Figures 6W–X). To further consider cristae structure, we used a metric known as the cristae score, which grades cristae from one to four based on their relative quality and quantity, with four representing "healthy" cristae (Lam et al. 2021; Eisner et al. 2017). The cristae score significantly decreased, validating loss of cristae integrity along with mitochondrial structure, which is evolutionarily conserved across both murine-derived myotubes and *Drosophila* (Figures 6T–Y).

Next, we examined MERC rearrangement. Using immunofluorescence, we stained mitochondria (mito-GFP; green), nuclei (DAPI; blue), and one of two MERC proteins, VDAC or phosphofurin acidic cluster sorting protein 2 (PACS2) (Figures 6Z–AA). In both cases, MARF KD increased VDAC and PACS2 levels, as well as the relative alignment with mitochondria (Figures 6Z–AA). These findings suggest that the ablation of MARF in *Drosophila* may increase MERCs through the localization of VDAC and PAC2 with mitochondria. Furthermore, MARK KD decreased the number of mitochondria and the aspect ratio (Figures 6AB–AC).

Discussion:

To our knowledge, studies of mitochondrial changes in human skeletal muscle throughout aging remain limited. Three-dimensional reconstructions of mitochondria showed that structural phenotypes in human skeletal muscle shift to a more compact state with age, concomitantly with the loss of proteins associated with mitochondrial and cristae dynamics. Because we observed a progressive decrease in muscle size with age, we suggest that age-related muscle atrophy in human skeletal muscle may arise in part due to mitochondrial loss of complexity and concomitant structural remodeling. This finding is further supported by the functional implications of limited exercise endurance among aged humans. Moreover, our data show that mitochondrial structure also rearranges in *Drosophila* with loss of MARF, the ortholog for MFN1 and MFN2. This finding suggests an evolutionarily conserved mechanism both *in vivo* and *in vitro* through which aging results in loss of MFN1 and MFN2, causing a decline in mitochondrial architectural integrity, with exercise serving as a potential therapy to restore mitochondrial structure and associated bioenergetics through increases in mitofusins. While our findings are based on general aging in skeletal muscle, they may carry significant translational implications for the development of therapies for sarcopenia. Based on these findings, there are several key promising areas that must be further explicated in the future.

Our key finding is that the 3D structures of intermyofibrillar mitochondria show a progressive decrease in complexity and reduced branching patterns, suggesting structural

remodeling caused by the aging process. Key genes associated with mitochondria and their contact sites are lost during the aging process. Past studies investigating human skeletal muscle 3D structure have shown that intermyofibrillar mitochondria are distinct from other mitochondrial subpopulations, such as subsarcolemmal mitochondria (Vincent et al. 2019), which are more interconnected than intermyofibrillar mitochondria (Dahl et al. 2015). Thus, investigating whether the structure of subsarcolemmal mitochondria changes during aging may offer insight into how mitochondrial subpopulations differentially respond to sarcopenia. Specifically, another study using FIB-SEM (Marshall, Damo, et al. 2023) showed that the 3D structure of Type I and Type II human skeletal muscle mitochondria also differed, with Type II having lower-volume mitochondria (Dahl et al. 2015). Notably, in sarcopenia, a preferential loss of Type II (fast-twitch) muscle fibers occurs, leading to an increased proportion of Type I (slow-twitch) fibers, for which previous studies have found higher mitochondrial fusion rates (Bellanti et al. 2021). Our present study did not allow for the differentiation of these fiber types; therefore, future investigations should consider the differential interplay between mitochondrial structure and exercise across these different fiber types and subpopulations.

Similarly, while we examined quadriceps muscles in this study, an interesting future avenue may be to compare these findings to the 3D structure of biceps and other skeletal muscle regions. Notably, we showed that, during aging, the reductions in upper body endurance are not as severe as those observed for lower body endurance (Figures 4G–H). This result may be due to differential mitochondrial structure remodeling with aging in different regions of skeletal muscle in humans; if this is the case, our finding that muscle atrophy is correlated with mitochondrial structure may be further supported. Similarly, while skeletal muscle mitochondria evidently directly impact muscle function, consideration of the wider neuromuscular system (Rygiel et al. 2016) suggests that modulation and changes in neuronal 3D mitochondrial structure may confer increased susceptibility to sarcopenia, which remains poorly elucidated.

One intriguing aspect of our study is the sex-dependent difference in muscle mass loss as individuals age. While male subjects showed a significant decrease in thigh CSA, females demonstrated an increase in femur CSA (Figure 1A). However, we noted a similar bone-to-thigh ratio for both sexes. Furthermore, there were slightly different changes in endurance with aging (Figure 4). Although the literature has referred to sex-specific aging impacts on sarcopenia (Tay et al. 2015), few studies have examined the interplay between these changes and mitochondrial dynamics in muscle tissue. Although we combined male and female samples in this study, future studies may further explore changes in the 3D structure of human skeletal muscle mitochondria based on sex.

Mitochondrial morphology loss occurs concomitantly with decreases in endurance and exercise strength during aging. Although the restoration of MFN2 levels following exercise suggests mitochondrial structure can be repaired, the limitations of *in vivo* studies make it difficult to predict exactly how mitochondrial structure may remodel in response to exercise. Generally, previous *in vivo* studies have suggested that exercise induces the same increase in MFN1 and MFN2 as we observed with our *in vitro* study (Axelrod et al. 2019; Huertas et al. 2019). Future studies must determine how mitochondrial structure remodels immediately following exercise and the long-term benefits of exercise regimens. While this remains difficult *in vivo*, the *in vitro* method for electrical pulse stimulation exercise may facilitate this study and further validate whether exercise alone can prevent mitochondrial remodeling. Previous studies have shown that murine mitochondria subjected to 3-hour acute exercise do not exhibit

alterations in size and morphology (Picard et al. 2013), yet few studies have investigated the effects on 3D morphology or differed exercise regimens. Thus, a promising future avenue is optimizing exercise regimens based on how they change mitochondrial dynamic proteins and associated mitochondrial 3D structure, which may offer a research-backed avenue to identify the types of exercise that provide the most therapeutic benefits to prevent sarcopenia.

Although MFN2 is a MERC tether protein (Basso et al. 2018; De Brito & Scorrano 2008), loss of MARF induced additional MERC formation. This finding suggests that MERCs may be formed by the upregulation of other MERC proteins, including VDAC and PACS2, as a compensatory mechanism during loss of MARF (Figure 6). Similarly, we noticed that while MFN2 was lost in human and murine samples with age, GRP75, IP_3R3, and VDAC3 were all increased, suggesting greater capacity for MERC formation (Figure 2). However, it remains unclear whether MFN2 is mediating this pathway. Notably, we recently showed that loss of OPA1, which occurs in the aging process (Tezze et al. 2017), also causes induction of ER stress and associated MERC tethering (Hinton et al. 2022). Therefore, it remains unclear whether MFN2 loss and OPA1 have pluralistic effects on MERC formation. It is possible that as mitochondria become more compact during aging (Figure 2), MERC tethering increases as a compensatory mechanism because the reduced branching and surface area limit the area for MERCs. Contrary to our findings, previous studies have found that exercise in murine models decreases MERC formation (Merle et al. 2019), potentially through mechanisms involving decreased ER stress (Kim et al. 2017). Thus, it remains unclear whether MERC formation is also involved in alterations in mitochondrial structure in exercise and aging. Therefore, future studies may seek to better elucidate how MERC phenotypes change in aged human skeletal muscle and determine whether these changes are independent of OPA1-mediated alterations.

An important future avenue is better exploring the role of FGF21 in sarcopenia. FGF21, as previously demonstrated, is a universal metabolism regulator that is important for modulating insulin sensitivity (Potthoff 2017). Notably, recent studies have revealed that FGF21 serum levels are increased in individuals with sarcopenia and are directly correlated with loss of muscle strength (Jung et al. 2021; Roh et al. 2021). FGF21 has a multitude of its principal inductors is ER stress, specifically through pathways involving ATF4 (Wan et al. 2014). Notably, ATF4 has also recently arisen as a key modulator of MERCs through OPA1-dependent pathways in skeletal muscle (Hinton et al. 2022). We also showed that ATF4 is increased with MARF KD (Supplemental Figure 5I). This finding suggests that FGF21 may be involved in MERC formation, which may have functional implications in the development of sarcopenia. However, few studies have investigated FGF21-dependent MERC formation. Mitofusins are understood to be required for glucose homeostasis and modulation of insulin sensitivity (Georgiadou et al. 2022; Sebastián et al. 2012). FGF21 may thus provide a mechanistic link through MFN-mediated development of sarcopenia through modulational of MERCs and functional implications of altered glucose metabolism due to mitochondrial structural rearrangement.

Our work also delved into the commonality of exercise and aging as producing similar phenotypes in some cases. Beyond FGF21, we also found that exercise affects IL6 and the immune response (Figure 4), which are observed to be hallmarks of aging (Ershler et al. 1993). While the literature is notably sparse on the molecular pathways that exercise influences to provide its anti-aging benefits, it is possible that immune responses are involved in these changes. This increase in IL-6 that occurs with exercise may occur through the same mechanism in which aging causes IL-6 uptick: ROS generation; however, the exact mechanism remains

poorly elucidated (Fischer 2006). Similarly, reduced oxidative stress may concomitantly decrease IL-6 (Lowes et al. 2013). Notably, PGC-1α expression, an important regulator of mitochondrial biogenesis, is linked to both IL-6 and aging, with loss of IL-6 having an inverse effect on PGC-1α levels (Bonda et al. 2017) and causing increased mitochondrial replication (Skuratovskaia et al. 2021). Beyond this, the IL-6 upregulates MFN1 to cause mitochondrial fusion, suggesting a potential mechanism through which exercise stimulates the mitochondrial fusion (Hou et al. 2023). It has been proposed that repeated exercise training can reduce age-related increases in IL-6 (Fischer 2006), suggesting exercise may be useful in modulating the immune response, but how age-dependent changes in IL-6 may contribute to mitochondrial remodeling remains an avenue for greater investigation.

Furthermore, independent from exercise, it is unclear whether MFN2 can be delivered to recapitulate the therapeutic effects of exercise on sarcopenia. Previously, loss of MFN1 and MFN2 was shown to impede exercise performance, suggesting that the age-related loss of endurance we observed is due to MFN2 (Bell et al. 2019). MFN1 and MFN2 also regulate glucose homeostasis through the determination of mtDNA content (Sidarala et al. 2022). Similarly, mtDNA content is decreased following exercise (Puente-Maestu et al. 2011). Given that high circulatory levels of mtDNA are associated with sarcopenia (Fan et al. 2022), this finding offers another potential mechanism through which exercise-mediated restoration of MFN2 protects against sarcopenia, but further investigation into how mtDNA content may alter mitochondrial structure is valuable. Regardless of the specific mechanism, measuring the therapeutic potential of MFN2 is a valuable future avenue. Notably, although MFN2 loss was associated with myocardial hypertrophy in cardiac tissue, gene delivery of an adenoviral vector encoding rat MFN2 proved to successfully protect against myocardial hypertrophy (Yu et al. 2011). However, it is unclear whether these techniques can successfully be applied to humans and if supplementation of MFN2 levels is an effective therapy independent of exercise. Furthermore, past studies have shown that active women do not have elevated MFN2 levels (Drummond et al. 2014), while other studies have shown the opposite, with immediate increases in MFN1 and MFN2 following exercise in athletes (Huertas et al. 2019). These results suggest that further research on the long-term effects on MFN2 protein levels following exercise is necessary.

Taken together, we found compelling evidence that several components related to mitochondrial dynamics, specifically proteins involved in mitochondrial fusion and fission, as well as the MICOS complex and MERCs, were altered during the aging process. This underscores our previous findings (Vue, Garza-Lopez, et al. 2023; Vue, Neikirk, et al. 2023), which show that, beyond only fusion and fission dynamics, the MICOS complex, MERCs, and mitochondrial 3D structure must all be considered in the aging process. Furthermore, our cross-species analysis using *Drosophila* models provided compelling evidence that the mechanisms we observed are evolutionarily conserved. While we are not the first to show that exercise increases MFN2 protein levels opposite to losses caused by aging (Koltai et al. 2012; Cartoni et al. 2005), the structural impacts of these changes have remained ambiguous. Although our findings further our understanding of age-dependent mitochondrial structure, the physiological implications of reduced mitochondrial complexity, the specific molecular mechanisms through which exercise delivers its benefits, and the evolutionary conservation of these mechanisms remain new avenues for therapeutic interventions to counteract the deleterious effects of aging.

Competing Interests Disclosure

All authors have no competing interests.

Financial Disclosures

This project was funded by the following agencies: National Institute of Health (NIH), NIDDK T-32, grant number DK007563, entitled Multidisciplinary Training in Molecular Endocrinology, to Z.V.; Integrated Training in Engineering and Diabetes, grant Number T32 DK101003; Burroughs Wellcome Fund Postdoctoral Enrichment Program #1022355 to D.S.; NSF grant MCB #2011577 to S.M.; NSF EES2112556, NSF EES1817282, NSF MCB1955975, and CZI Science Diversity Leadership grant number 2022-253614 from the Chan Zuckerberg Initiative DAF, an advised fund of the Silicon Valley Community Foundation to S.D.; the UNCF/Bristol-Myers Squibb E.E. Just Faculty Fund, Career Award at the Scientific Interface (CASI Award) from the Burroughs Welcome Fund (BWF) ID # 1021868.01, BWF Ad-hoc Award, NIH Small Research Pilot Subaward 5R25HL106365-12 from the National Institutes of Health PRIDE Program, DK020593, Vanderbilt Diabetes and Research Training Center for DRTC Alzheimer's Disease Pilot & Feasibility Program, CZI Science Diversity Leadership grant number 2022-253529 from the Chan Zuckerberg Initiative DAF, an advised fund of the Silicon Valley Community Foundation to A.H.J.; NIH grant HD090061 and the Department of Veterans Affairs Office of Research Award I01 BX005352 to J.G.; NIH grants R21DK119879 and R01DK-133698, American Heart Association Grant 16SDG27080009, and an American Society of Nephrology KidneyCure Transition to Independence Grant to C.R.W. Additional support was provided by the Vanderbilt Institute for Clinical and Translational Research program, supported by the National Center for Research Resources, Grant UL1 RR024975–01, the National Center for Advancing Translational Sciences, Grant 2 UL1 TR000445–06, and the Cell Imaging Shared Resource. The contents are solely the responsibility of the authors and do not necessarily represent the official view of the NIH. The funders had no role in the study design, data collection and analysis, decision to publish, or preparation of the manuscript.

Data Sharing and Open Access

All data are available upon request to the corresponding author.

References:

Axelrod CL, Fealy CE, Mulya A & Kirwan JP (2019) Exercise training remodels human skeletal muscle mitochondrial fission and fusion machinery towards a pro-elongation phenotype. *Acta Physiologica* 225, e13216.

Bartsakoulia M, Pyle A, Troncoso-Chandía D, Vial-Brizzi J, Paz-Fiblas MV, Duff J, Griffin H, Boczonadi V, Lochmüller H, Kleinle S, Chinnery PF, Grünert S, Kirschner J, Eisner V & Horvath R (2018) A novel mechanism causing imbalance of mitochondrial fusion and fission in human myopathies. *Human Molecular Genetics* 27, 1186–1195.

Basso V, Marchesan E, Peggion C, Chakraborty J, von Stockum S, Giacomello M, Ottolini D, Debattisti V, Caicci F, Tasca E, Pegoraro V, Angelini C, Antonini A, Bertoli A, Brini M & Ziviani E (2018) Regulation of ER-mitochondria contacts by Parkin via Mfn2. *Pharmacol Res* 138, 43–56.

Beavers KM, Brinkley TE & Nicklas BJ (2010) Effect of exercise training on chronic inflammation. *Clinica Chimica Acta* 411, 785–793.

Bell MB, Bush Z, McGinnis GR & Rowe GC (2019) Adult skeletal muscle deletion of Mitofusin 1 and 2 impedes exercise performance and training capacity. *J Appl Physiol (1985)* 126, 341–353.

Bellanti F, Lo Buglio A & Vendemiale G (2021) Mitochondrial Impairment in Sarcopenia. *Biology (Basel)* 10, 31.

Beneke R, Neuerburg J & Bohndorf K (1991) Muscle cross-section measurement by magnetic resonance imaging. *Eur J Appl Physiol Occup Physiol* 63, 424–429.

Beregi E, Regius O, Hüttl T & Göbl Z (1988) Age-related changes in the skeletal muscle cells. *Z Gerontol* 21, 83–86.

Bonda TA, Dziemidowicz M, Sokołowska M, Szynaka B, Waszkiewicz E, Winnicka MM & Kamiński KA (2017) Interleukin-6 Affects Aging-Related Changes of the PPARα-PGC-1α Axis in the Myocardium. *Journal of Interferon & Cytokine Research* 37, 513–521.

Boudina S, Sena S, Theobald H, Sheng X, Wright JJ, Hu XX, Aziz S, Johnson JI, Bugger H, Zaha VG & Abel ED (2007) Mitochondrial energetics in the heart in obesity-related diabetes: direct evidence for increased uncoupled respiration and activation of uncoupling proteins. *Diabetes* 56, 2457–2466.

Bratic A & Larsson N-G (2013) The role of mitochondria in aging. *The Journal of clinical investigation* 123, 951–957.

Brunyanszki A, Erdelyi K, Szczesny B, Olah G, Salomao R, Herndon DN & Szabo C (2015) Upregulation and Mitochondrial Sequestration of Hemoglobin Occur in Circulating Leukocytes during Critical Illness, Conferring a Cytoprotective Phenotype. *Mol Med* 21, 666–675.

Bustos G, Cruz P, Lovy A & Cárdenas C (2017) Endoplasmic reticulum–mitochondria calcium communication and the regulation of mitochondrial metabolism in cancer: a novel potential target. *Frontiers in oncology* 7, 199.

Callahan DM, Bedrin NG, Subramanian M, Berking J, Ades PA, Toth MJ & Miller MS (2014) Age-related structural alterations in human skeletal muscle fibers and mitochondria are sex specific: relationship to single-fiber function. *Journal of Applied Physiology* 116, 1582–1592.

Campo A del, Contreras-Hernández I, Castro-Sepúlveda M, Campos CA, Figueroa R, Tevy MF, Eisner V, Casas M & Jaimovich E (2018) Muscle function decline and mitochondria changes in middle age precede sarcopenia in mice. *Aging* 10, 34–55.

Cartee GD, Hepple RT, Bamman MM & Zierath JR (2016) Exercise promotes healthy aging of skeletal muscle. *Cell metabolism* 23, 1034–1047.

Cartoni R, Léger B, Hock MB, Praz M, Crettenand A, Pich S, Ziltener J-L, Luthi F, Dériaz O, Zorzano A, Gobelet C, Kralli A & Russell AP (2005) Mitofusins 1/2 and ERRα expression are increased in human skeletal muscle after physical exercise. *J Physiol* 567, 349–358.

Chan DC (2012) Fusion and fission: interlinked processes critical for mitochondrial health. *Annual review of genetics* 46, 265–287.

Chen H, Chomyn A & Chan DC (2005) Disruption of fusion results in mitochondrial heterogeneity and dysfunction. *J Biol Chem* 280, 26185–26192.

Chen H, Detmer SA, Ewald AJ, Griffin EE, Fraser SE & Chan DC (2003) Mitofusins Mfn1 and Mfn2 coordinately regulate mitochondrial fusion and are essential for embryonic development. *J Cell Biol* 160, 189–200.

Coen PM, Musci RV, Hinkley JM & Miller BF (2019) Mitochondria as a Target for Mitigating Sarcopenia. *Front Physiol* 9, 1883.

Cogliati S, Enriquez JA & Scorrano L (2016) Mitochondrial cristae: where beauty meets functionality. *Trends in biochemical sciences* 41, 261–273.

Cosson P, Marchetti A, Ravazzola M & Orci L (2012) Mitofusin-2 independent juxtaposition of endoplasmic reticulum and mitochondria: an ultrastructural study.

Courson JA, Landry PT, Do T, Spehlmann E, Lafontant PJ, Patel N, Rumbaut RE & Burns AR (2021) Serial Block-Face Scanning Electron Microscopy (SBF-SEM) of Biological Tissue Samples. *J Vis Exp*, 10.3791/62045.

Crabtree A, Neikirk K, Marshall AG, Vang L, Whiteside AJ, Williams Q, Altamura CT, Owens TC, Stephens D, Shao B, Koh A, Killion M, Lopez EG, Lam J, Rodriguez B, Mungai M, Stanley J, Dean ED, Koh H-J, Gaddy JA, Scudese E, Sweetwyne MT, Davis J, Zaganjor E, Murray SA, Katti P, Damo SM, Vue Z & Hinton A (2023) Defining Mitochondrial Cristae Morphology Changes Induced by Aging in Brown Adipose Tissue. *Adv Biol (Weinh)*, e2300186.

Crane JD, Devries MC, Safdar A, Hamadeh MJ & Tarnopolsky MA (2010) The Effect of Aging on Human Skeletal Muscle Mitochondrial and Intramyocellular Lipid Ultrastructure. *The Journals of Gerontology: Series A* 65A, 119–128.

Dahl R, Larsen S, Dohlmann TL, Qvortrup K, Helge JW, Dela F & Prats C (2015) Three-dimensional reconstruction of the human skeletal muscle mitochondrial network as

a tool to assess mitochondrial content and structural organization. *Acta Physiol (Oxf)* 213, 145–155.

De Brito OM & Scorrano L (2008) Mitofusin 2 tethers endoplasmic reticulum to mitochondria. *Nature* 456, 605–610.

Dong F, Zhu M, Zheng F & Fu C (2022) Mitochondrial fusion and fission are required for proper mitochondrial function and cell proliferation in fission yeast. *FEBS J* 289, 262–278.

Dorn GW, Clark CF, Eschenbacher WH, Kang M-Y, Engelhard JT, Warner SJ, Matkovich SJ & Jowdy CC (2011) MARF and Opa1 control mitochondrial and cardiac function in Drosophila. *Circ Res* 108, 12–17.

Drummond MJ, Addison O, Brunker L, Hopkins PN, McClain DA, LaStayo PC & Marcus RL (2014) Downregulation of E3 Ubiquitin Ligases and Mitophagy-Related Genes in Skeletal Muscle of Physically Inactive, Frail Older Women: A Cross-Sectional Comparison. *The Journals of Gerontology: Series A* 69, 1040–1048.

Eisner V, Cupo RR, Gao E, Csordás G, Slovinsky WS, Paillard M, Cheng L, Ibetti J, Chen SRW, Chuprun JK, Hoek JB, Koch WJ & Hajnóczky G (2017) Mitochondrial fusion dynamics is robust in the heart and depends on calcium oscillations and contractile activity. *Proc Natl Acad Sci U S A* 114, E859–E868.

Ershler WB, Sun WH, Binkley N, Gravenstein S, Volk MJ, Kamoske G, Klopp RG, Roecker EB, Daynes RA & Weindruch R (1993) Interleukin-6 and aging: blood levels and mononuclear cell production increase with advancing age and in vitro production is modifiable by dietary restriction. *Lymphokine Cytokine Res* 12, 225–230.

Evers-van Gogh IJA, Alex S, Stienstra R, Brenkman AB, Kersten S & Kalkhoven E (2015) Electric Pulse Stimulation of Myotubes as an In Vitro Exercise Model: Cell-Mediated and Non-Cell-Mediated Effects. *Sci Rep* 5, 10944.

Fan Z, Yang J, Guo Y, Liu Y & Zhong X (2022) Altered levels of circulating mitochondrial DNA in elderly people with sarcopenia: Association with mitochondrial impairment. *Experimental Gerontology* 163, 111802.

Filippin LI, Teixeira VN de O, da Silva MPM, Miraglia F & da Silva FS (2015) Sarcopenia: a predictor of mortality and the need for early diagnosis and intervention. *Aging Clin Exp Res* 27, 249–254.

Fischer CP (2006) Interleukin-6 in acute exercise and training: what is the biological relevance. *Exerc immunol rev* 12, 41.

Frey TG & Mannella CA (2000) The internal structure of mitochondria. *Trends in biochemical sciences* 25, 319–324.

Gaffney CJ, Pollard A, Barratt TF, Constantin-Teodosiu D, Greenhaff PL & Szewczyk NJ (2018) Greater loss of mitochondrial function with ageing is associated with earlier onset of sarcopenia in C. elegans. *Aging (Albany NY)* 10, 3382–3396.

Gallo V, Ciotti MT, Coletti A, Aloisi F & Levi G (1982) Selective release of glutamate from cerebellar granule cells differentiating in culture. *Proc Natl Acad Sci U S A* 79, 7919–7923.

Garza-Lopez E, Vue Z, Katti P, Neikirk K, Biete M, Lam J, Beasley HK, Marshall AG, Rodman TA, Christensen TA, Salisbury JL, Vang L, Mungai M, AshShareef S, Murray SA, Shao J, Streeter J, Glancy B, Pereira RO, Abel ED & Hinton A (2022) Protocols for Generating Surfaces and Measuring 3D Organelle Morphology Using Amira. *Cells* 11, 65.

Georgiadou E, Muralidharan C, Martinez M, Chabosseau P, Akalestou E, Tomas A, Wern FYS, Stylianides T, Wretlind A, Legido-Quigley C, Jones B, Lopez-Noriega L, Xu Y, Gu G, Alsabeeh N, Cruciani-Guglielmacci C, Magnan C, Ibberson M, Leclerc I, Ali Y, Soleimanpour SA, Linnemann AK, Rodriguez TA & Rutter GA (2022) Mitofusins Mfn1 and Mfn2 Are Required to Preserve Glucose- but Not Incretin-Stimulated β-Cell Connectivity and Insulin Secretion. *Diabetes* 71, 1472–1489.

Glancy B, Kim Y, Katti P & Willingham TB (2020) The Functional Impact of Mitochondrial Structure Across Subcellular Scales. *Frontiers in Physiology* 11. Available at: https://www.frontiersin.org/articles/10.3389/fphys.2020.541040 [Accessed December 16, 2022].

Goodwin ML, Harris JE, Hernández A & Gladden LB (2007) Blood Lactate Measurements and Analysis during Exercise: A Guide for Clinicians. *Journal of diabetes science and technology (Online)* 1, 558.

Greenlund LJS & Nair KS (2003) Sarcopenia—consequences, mechanisms, and potential therapies. *Mechanisms of Ageing and Development* 124, 287–299.

Han S, Zhao F, Hsia J, Ma X, Liu Y, Torres S, Fujioka H & Zhu X (2021) The role of Mfn2 in the structure and function of endoplasmic reticulum-mitochondrial tethering in vivo. *J Cell Sci* 134, jcs253443.

Hara Y, Yuk F, Puri R, Janssen WGM, Rapp PR & Morrison JH (2014) Presynaptic mitochondrial morphology in monkey prefrontal cortex correlates with working memory and is improved with estrogen treatment. *Proceedings of the National Academy of Sciences* 111, 486–491.

Hepple RT (2014) Mitochondrial Involvement and Impact in Aging Skeletal Muscle. *Frontiers in Aging Neuroscience* 6. Available at: https://www.frontiersin.org/articles/10.3389/fnagi.2014.00211 [Accessed October 24, 2023].

Hinton A, Katti P, Christensen TA, Mungai M, Shao J, Zhang L, Trushin S, Alghanem A, Jaspersen A, Geroux RE, Neikirk K, Biete M, Lopez EG, Shao B, Vue Z, Vang L, Beasley HK, Marshall AG, Stephens D, Damo S, Ponce J, Bleck CKE, Hicsasmaz I, Murray SA, Edmonds RAC, Dajles A, Koo YD, Bacevac S, Salisbury JL, Pereira RO, Glancy B, Trushina E & Abel ED (2023) A Comprehensive Approach to Sample Preparation for Electron Microscopy and the Assessment of Mitochondrial Morphology in Tissue and Cultured Cells. *Adv Biol (Weinh)*, e2200202.

Hinton A, Katti P, Mungai M, Hall D, Koval O, Shao J, Vue Z, Christensen TA, Lopez EG, Rostami R, Neikirk K, Lam J, Alghanem A, Ponce J, Hicsasmaz I, Streeter J, Schickling B, Bacevac S, Grueter C, Marshall A, Beasley HK, DoKoo Y, Bodine S, Nava NGR, Quintana A, Trushina E, Weatherford E, Murray SA, Salisbury J, Song L-S, Grumbach I, Exil V, Pereira RO, Glancy B & Abel ED (2022) OPA1 Downregulation in Skeletal Muscle Induces MERC formation in an ATF4-Dependent Manner. , 2022.09.12.507669.

Hou D, Zheng X, Cai D, You R, Liu J, Wang X, Liao X, Tan M, Lin L, Wang J, Zhang S & Huang H (2023) Interleukin-6 Facilitates Acute Myeloid Leukemia Chemoresistance via Mitofusin 1–Mediated Mitochondrial Fusion. *Molecular Cancer Research*, OF1–OF13.

Huertas JR, Ruiz-Ojeda FJ, Plaza-Díaz J, Nordsborg NB, Martín-Albo J, Rueda-Robles A & Casuso RA (2019) Human muscular mitochondrial fusion in athletes during exercise. *FASEB J* 33, 12087–12098.

Jung H-W, Park JH, Kim DA, Jang I-Y, Park SJ, Lee JY, Lee S, Kim JH, Yi H-S, Lee E & Kim B-J (2021) Association between serum FGF21 level and sarcopenia in older adults. *Bone* 145, 115877.

Katti P, Rai M, Srivastava S & Nongthomba U (2021) Marf-mediated mitochondrial fusion is imperative for the development and functioning of indirect flight muscles (IFMs) in drosophila. *Experimental Cell Research* 399, 112486.

Kim K, Ahn N, Jung S & Park S (2017) Effects of intermittent ladder-climbing exercise training on mitochondrial biogenesis and endoplasmic reticulum stress of the cardiac muscle in obese middle-aged rats. *Korean J Physiol Pharmacol* 21, 633–641.

Kim TN & Choi KM (2013) Sarcopenia: Definition, Epidemiology, and Pathophysiology. *J Bone Metab* 20, 1–10.

Koltai E, Hart N, Taylor AW, Goto S, Ngo JK, Davies KJA & Radak Z (2012) Age-associated declines in mitochondrial biogenesis and protein quality control factors are minimized by exercise training. *American Journal of Physiology-Regulatory, Integrative and Comparative Physiology* 303, R127–R134.

Lam J, Katti P, Biete M, Mungai M, AshShareef S, Neikirk K, Garza Lopez E, Vue Z, Christensen TA, Beasley HK, Rodman TA, Murray SA, Salisbury JL, Glancy B,

Shao J, Pereira RO, Abel ED & Hinton A (2021) A Universal Approach to Analyzing Transmission Electron Microscopy with ImageJ. *Cells* 10, 2177.

Lambernd S, Taube A, Schober A, Platzbecker B, Görgens SW, Schlich R, Jeruschke K, Weiss J, Eckardt K & Eckel J (2012) Contractile activity of human skeletal muscle cells prevents insulin resistance by inhibiting pro-inflammatory signalling pathways. *Diabetologia* 55, 1128–1139.

Leal NS, Schreiner B, Pinho CM, Filadi R, Wiehager B, Karlström H, Pizzo P & Ankarcrona M (2016) Mitofusin-2 knockdown increases ER–mitochondria contact and decreases amyloid β-peptide production. *Journal of Cellular and Molecular Medicine* 20, 1686–1695.

Leduc-Gaudet J-P, Picard M, Pelletier FS-J, Sgarioto N, Auger M-J, Vallée J, Robitaille R, St-Pierre DH & Gouspillou G (2015) Mitochondrial morphology is altered in atrophied skeletal muscle of aged mice. *Oncotarget* 6, 17923–17937.

Liao Y, Wang J, Jaehnig EJ, Shi Z & Zhang B (2019) WebGestalt 2019: gene set analysis toolkit with revamped UIs and APIs. *Nucleic Acids Res* 47, W199–W205.

Liu X & Hajnóczky G (2011) Altered fusion dynamics underlie unique morphological changes in mitochondria during hypoxia–reoxygenation stress. *Cell Death Differ* 18, 1561–1572.

Lowes DA, Webster NR, Murphy MP & Galley HF (2013) Antioxidants that protect mitochondria reduce interleukin-6 and oxidative stress, improve mitochondrial function, and reduce biochemical markers of organ dysfunction in a rat model of acute sepsis. *BJA: British Journal of Anaesthesia* 110, 472–480.

Maden-Wilkinson TM, McPhee JS, Rittweger J, Jones DA & Degens H (2014) Thigh muscle volume in relation to age, sex and femur volume. *Age (Dordr)* 36, 383–393.

Mare TA, Treacher DF, Shankar-Hari M, Beale R, Lewis SM, Chambers DJ & Brown KA (2015) The diagnostic and prognostic significance of monitoring blood levels of immature neutrophils in patients with systemic inflammation. *Crit Care* 19, 57.

Marshall AG, Damo SM & Hinton A (2023) Revisiting focused ion beam scanning electron microcopy. *Trends in Biochemical Sciences* 0. Available at: https://www.cell.com/trends/biochemical-sciences/abstract/S0968-0004(23)00056-7 [Accessed April 7, 2023].

Marshall AG, Krystofiak E, Damo SM & Hinton A (2023) Correlative light-electron microscopy: integrating dynamics to structure. *Trends Biochem Sci*, S0968-0004(23)00127-5.

Marshall AG, Neikirk K, Stephens DC, Vang L, Vue Z, Beasley HK, Crabtree A, Scudese E, Lopez EG, Shao B, Krystofiak E, Rutledge S, Davis J, Murray SA, Damo SM, Katti

P & Hinton A (2023) Serial Block Face-Scanning Electron Microscopy as a Burgeoning Technology. *Adv Biol (Weinh)*, e2300139.

Martinez BP, Batista AKMS, Gomes IB, Olivieri FM, Camelier FWR & Camelier AA (2015) Frequency of sarcopenia and associated factors among hospitalized elderly patients. *BMC Musculoskeletal Disorders* 16, 108.

Merle A, Jollet M, Britto FA, Goustard B, Bendridi N, Rieusset J, Ollendorff V & Favier FB (2019) Endurance exercise decreases protein synthesis and ER-mitochondria contacts in mouse skeletal muscle. *Journal of Applied Physiology* 127, 1297–1306.

Mul JD, Stanford KI, Hirshman MF & Goodyear LJ (2015) Exercise and Regulation of Carbohydrate Metabolism. *Prog Mol Biol Transl Sci* 135, 17–37.

Mustafi D, Kikano S & Palczewski K (2014) Serial Block Face□Scanning Electron Microscopy: A Method to Study Retinal Degenerative Phenotypes. *Current protocols in mouse biology* 4, 197–204.

Nalbandian M & Takeda M (2016) Lactate as a Signaling Molecule That Regulates Exercise-Induced Adaptations. *Biology (Basel)* 5, 38.

Neikirk K, Vue Z, Katti P, Rodriguez BI, Omer S, Shao J, Christensen T, Garza Lopez E, Marshall A, Palavicino-Maggio CB, Ponce J, Alghanem AF, Vang L, Barongan T, Beasley HK, Rodman T, Stephens D, Mungai M, Correia M, Exil V, Damo S, Murray SA, Crabtree A, Glancy B, Pereira RO, Abel ED & Hinton Jr. AO (2023) Systematic Transmission Electron Microscopy-Based Identification and 3D Reconstruction of Cellular Degradation Machinery. *Advanced Biology* 7, 2200221.

Ngoh GA, Papanicolaou KN & Walsh K (2012) Loss of mitofusin 2 promotes endoplasmic reticulum stress. *J Biol Chem* 287, 20321–20332.

Pandya CD, Vekaria H, Joseph B, Slone SA, Gensel JC, Sullivan PG & Miller BA (2021) Hemoglobin induces oxidative stress and mitochondrial dysfunction in oligodendrocyte progenitor cells. *Translational Research* 231, 13–23.

Parra V, Verdejo HE, Iglewski M, del Campo A, Troncoso R, Jones D, Zhu Y, Kuzmicic J, Pennanen C, Lopez□Crisosto C, Jaña F, Ferreira J, Noguera E, Chiong M, Bernlohr DA, Klip A, Hill JA, Rothermel BA, Abel ED, Zorzano A & Lavandero S (2013) Insulin Stimulates Mitochondrial Fusion and Function in Cardiomyocytes via the Akt-mTOR-NFκB-Opa-1 Signaling Pathway. *Diabetes* 63, 75–88.

Patra M, Mahata SK, Padhan DK & Sen M (2016) CCN6 regulates mitochondrial function. *Journal of Cell Science* 129, 2841–2851.

Peggion C, Massimino ML, Bonadio RS, Lia F, Lopreiato R, Cagnin S, Calì T & Bertoli A (2021) Regulation of Endoplasmic Reticulum–Mitochondria Tethering and Ca2+ Fluxes by TDP-43 via GSK3β. *Int J Mol Sci* 22, 11853.

Pereira RO, Marti A, Olvera AC, Tadinada SM, Bjorkman SH, Weatherford ET, Morgan DA, Westphal M, Patel PH, Kirby AK, Hewezi R, Bùi Trân W, García-Peña LM, Souvenir RA, Mittal M, Adams CM, Rahmouni K, Potthoff MJ & Abel ED (2021) OPA1 deletion in brown adipose tissue improves thermoregulation and systemic metabolism via FGF21 J. K. Elmquist & D. E. James, eds. *eLife* 10, e66519.

Pereira RO, Tadinada SM, Zasadny FM, Oliveira KJ, Pires KMP, Olvera A, Jeffers J, Souvenir R, Mcglauflin R & Seei A (2017) OPA 1 deficiency promotes secretion of FGF 21 from muscle that prevents obesity and insulin resistance. *The EMBO journal* 36, 2126–2145.

Phu S, Boersma D & Duque G (2015) Exercise and Sarcopenia. *Journal of Clinical Densitometry* 18, 488–492.

Picard M, Gentil BJ, McManus MJ, White K, St. Louis K, Gartside SE, Wallace DC & Turnbull DM (2013) Acute exercise remodels mitochondrial membrane interactions in mouse skeletal muscle. *Journal of Applied Physiology* 115, 1562–1571.

Potthoff MJ (2017) FGF21 and metabolic disease in 2016: A new frontier in FGF21 biology. *Nat Rev Endocrinol* 13, 74–76.

Puente-Maestu L, Lázaro A, Tejedor A, Camaño S, Fuentes M, Cuervo M, Navarro BO & Agustí A (2011) Effects of exercise on mitochondrial DNA content in skeletal muscle of patients with COPD. *Thorax* 66, 121–127.

Roh E, Hwang SY, Yoo HJ, Baik SH, Cho B, Park YS, Kim HJ, Lee S-G, Kim BJ, Jang HC, Kim M, Won CW & Choi KM (2021) Association of plasma FGF21 levels with muscle mass and muscle strength in a national multicentre cohort study: Korean Frailty and Aging Cohort Study. *Age and Ageing* 50, 1971–1978.

Rygiel KA, Picard M & Turnbull DM (2016) The ageing neuromuscular system and sarcopenia: a mitochondrial perspective. *The Journal of Physiology* 594, 4499–4512.

Safiulina D, Veksler V, Zharkovsky A & Kaasik A (2006) Loss of mitochondrial membrane potential is associated with increase in mitochondrial volume: physiological role in neurones. *J Cell Physiol* 206, 347–353.

Schneider CA, Rasband WS & Eliceiri KW (2012) NIH Image to ImageJ: 25 years of image analysis. *Nature methods* 9, 671–675.

Sebastián D, Hernández-Alvarez MI, Segalés J, Sorianello E, Muñoz JP, Sala D, Waget A, Liesa M, Paz JC & Gopalacharyulu P (2012) Mitofusin 2 (Mfn2) links mitochondrial and endoplasmic reticulum function with insulin signaling and is essential for normal glucose homeostasis. *Proceedings of the National Academy of Sciences* 109, 5523–5528.

Seo AY, Joseph A-M, Dutta D, Hwang JCY, Aris JP & Leeuwenburgh C (2010) New insights into the role of mitochondria in aging: mitochondrial dynamics and more. *Journal of Cell Science* 123, 2533–2542.

Sidarala V, Zhu J, Levi-D'Ancona E, Pearson GL, Reck EC, Walker EM, Kaufman BA & Soleimanpour SA (2022) Mitofusin 1 and 2 regulation of mitochondrial DNA content is a critical determinant of glucose homeostasis. *Nat Commun* 13, 2340.

Skuratovskaia D, Komar A, Vulf M, Quang HV, Shunkin E, Volkova L, Gazatova N, Zatolokin P & Litvinova L (2021) IL-6 Reduces Mitochondrial Replication, and IL-6 Receptors Reduce Chronic Inflammation in NAFLD and Type 2 Diabetes. *International Journal of Molecular Sciences* 22, 1774.

Sousa AS, Guerra RS, Fonseca I, Pichel F & Amaral TF (2015) Sarcopenia among hospitalized patients – A cross-sectional study. *Clinical Nutrition* 34, 1239–1244.

Stephens DC, Mungai M, Crabtree A, Beasley HK, Garza-Lopez E, Vang L, Neikirk K, Vue Z, Vue N, Marshall AG, Turner K, Shao J, Sarker B, Murray S, Gaddy JA, Davis J, Damo SM & Hinton AO (2023) Components of Isolated Skeletal Muscle Differentiated Through Antibody Validation. , 2023.05.20.541600. Available at: https://www.biorxiv.org/content/10.1101/2023.05.20.541600v1 [Accessed August 5, 2023].

Taaffe DR (2020) Sarcopenia: exercise as a treatment strategy. *Australian Family Physician* 35. Available at: https://search.informit.org/doi/abs/10.3316/INFORMIT.364765713154678 [Accessed October 22, 2023].

Tay L, Ding YY, Leung BP, Ismail NH, Yeo A, Yew S, Tay KS, Tan CH & Chong MS (2015) Sex-specific differences in risk factors for sarcopenia amongst community-dwelling older adults. *Age (Dordr)* 37, 121.

Tezze C, Romanello V, Desbats MA, Fadini GP, Albiero M, Favaro G, Ciciliot S, Soriano ME, Morbidoni V, Cerqua C, Loefler S, Kern H, Franceschi C, Salvioli S, Conte M, Blaauw B, Zampieri S, Salviati L, Scorrano L & Sandri M (2017) Age-Associated Loss of OPA1 in Muscle Impacts Muscle Mass, Metabolic Homeostasis, Systemic Inflammation, and Epithelial Senescence. *Cell Metab* 25, 1374-1389.e6.

Vendelin M, Béraud N, Guerrero K, Andrienko T, Kuznetsov AV, Olivares J, Kay L & Saks VA (2005) Mitochondrial regular arrangement in muscle cells: a "crystal-like" pattern. *American Journal of Physiology-Cell Physiology* 288, C757–C767.

Vincent AE, White K, Davey T, Philips J, Ogden RT, Lawless C, Warren C, Hall MG, Ng YS, Falkous G, Holden T, Deehan D, Taylor RW, Turnbull DM & Picard M (2019) Quantitative 3D Mapping of the Human Skeletal Muscle Mitochondrial Network. *Cell Reports* 26, 996-1009.e4.

Vue Z, Garza-Lopez E, Neikirk K, Katti P, Vang L, Beasley H, Shao J, Marshall AG, Crabtree A, Murphy AC, Jenkins BC, Prasad P, Evans C, Taylor B, Mungai M, Killion M, Stephens D, Christensen TA, Lam J, Rodriguez B, Phillips MA, Daneshgar N, Koh H-J, Koh A, Davis J, Devine N, Muhammod S, Scudese E, Arnold KR, Chavarin VV, Robinson RD, Chakraborty M, Gaddy JA, Sweetwyne M, Wilson G, Zaganjor E, Kezos J, Dondi C, Reddy AK, Glancy B, Kirabo A, Quintana AM, Dai D-F, Ocorr K, Murray SA, Damo SM, Exil V, Riggs B, Mobley BC, Gomez JA, McReynolds MR & Hinton A (2023) 3D Reconstruction of Murine Mitochondria Exhibits Changes in Structure Across Aging Linked to the MICOS Complex. *Aging Cell*, 2022.03.22.485341. Available at: https://www.biorxiv.org/content/10.1101/2022.03.22.485341v10 [Accessed September 20, 2023].

Vue Z, Neikirk K, Vang L, Garza-Lopez E, Christensen TA, Shao J, Lam J, Beasley HK, Marshall AG, Crabtree A, Anudokem J, Rodriguez B, Kirk B, Bacevac S, Barongan T, Shao B, Stephens DC, Kabugi K, Koh H-J, Koh A, Evans CS, Taylor B, Reddy AK, Miller-Fleming T, Actkins KV, Zaganjor E, Daneshgar N, Murray SA, Mobley BC, Damo S, Gaddy JA, Riggs B, Wanjalla C, Kirabo A, McReynolds M, Gomez JA, Phillips MA, Exil V, Dai D-F & Hinton A (2023) Three-Dimensional Mitochondria Reconstructions of Murine Cardiac Muscle Changes in Size Across Aging. *American Journal of Physiology-Heart and Circulatory Physiology*. Available at: https://journals.physiology.org/doi/abs/10.1152/ajpheart.00202.2023 [Accessed September 20, 2023].

Wan X, Lu X, Xiao Y, Lin Y, Zhu H, Ding T, Yang Y, Huang Y, Zhang Y, Liu Y-L, Xu Z, Xiao J & Li X (2014) ATF4- and CHOP-Dependent Induction of FGF21 through Endoplasmic Reticulum Stress. *BioMed Research International* 2014, e807874.

Xu J, Stanislaus S, Chinookoswong N, Lau YY, Hager T, Patel J, Ge H, Weiszmann J, Lu S-C, Graham M, Busby J, Hecht R, Li Y-S, Li Y, Lindberg R & Véniant MM (2009) Acute glucose-lowering and insulin-sensitizing action of FGF21 in insulin-resistant mouse models—association with liver and adipose tissue effects. *American Journal of Physiology-Endocrinology and Metabolism* 297, E1105–E1114.

Xuefei Y, Xinyi Z, Qing C, Dan Z, Ziyun L, Hejuan Z, Xindong X & Jianhua F (2021) Effects of Hyperoxia on Mitochondrial Homeostasis: Are Mitochondria the Hub for Bronchopulmonary Dysplasia? *Front Cell Dev Biol* 9, 642717.

Yu H, Guo Y, Mi L, Wang X, Li L & Gao W (2011) Mitofusin 2 inhibits angiotensin II-induced myocardial hypertrophy. *J Cardiovasc Pharmacol Ther* 16, 205–211.

Yung RL (2000) CHANGES IN IMMUNE FUNCTION WITH AGE. *Rheumatic Disease Clinics of North America* 26, 455–473.

Zhang X, Gregg EW, Williamson DF, Barker LE, Thomas W, Bullard KM, Imperatore G, Williams DE & Albright AL (2010) A1C Level and Future Risk of Diabetes: A Systematic Review. *Diabetes Care* 33, 1665–1673.

Figures:

Figure 1. Comparative Analyses of Musculoskeletal Characteristics in Young and Old Subjects Differentiated by Sex. Cross-sectional imaging of musculature and skeletal anatomy data from (A) females under 50 years old (aged 8–41 years old; n = 7), (B) females over 50 years old (aged 57–79 years old; n = 13), (C) males under 50 years old (aged 19–48 years old; n = 10), and (D) males over 50 years old (aged 67–85 years old; n = 10). (E) Thigh cross-sectional area (CSA) measurements for females and (E’) males, with data for young and old subjects represented by blue and purple bars, respectively. (F) Femur CSA measurements for females and (F’) males. (G) Ratio of thigh CSA and femur CSA for females and (G’) males. Individual data points indicating separate individuals (Supplemental File 1) are represented by dots on the bar graphs. (E–G) Mann–Whitney tests were used for statistical analysis. Statistical significance is denoted as ns (not significant), *$p < 0.05$, and **$p < 0.01$.

Figure 2. Changes in Mitochondrial Dynamics and Structure with Aging in Human Skeletal Muscle. (A–D) Quantified differences in mRNA fold changes, as determined by quantitative PCR, of various mitochondrial dynamic proteins, (E–G) mitochondrial contact site and cristae organizing system (MICOS) proteins, and (H–J) mitochondrial–endoplasmic reticulum contact site proteins. Parameters are compared between the young and old groups. (K) Workflow of serial block-face scanning electron microscopy (SBF-SEM) manual contour reconstruction to recreate 3D mitochondrial structure from young and old human samples. The workflow depicts SBF-SEM, allowing for orthoslice alignment, subsequent manual segmentation of orthoslices, and ultimately, 3D reconstructions of mitochondria. (L) Differences in orthoslice mitochondrial structure between young and (L)’ old human skeletal muscle, with a scale bar of 2 μm. (M) Overlaid view of the segmented mitochondria on the orthoslice, emphasizing distinct mitochondrial shapes and distributions observed with 3D reconstruction in young and (M’) older subjects. (N) 3D reconstructed images of isolated mitochondria from young and (N’) older subjects. (O) Differences in mitochondrial volume, (P) mitochondrial area, and (Q) perimeter between the young and old groups. (A–J) Each dot represents an independent experimental run or (O–Q) average of all mitochondria quantifications in each region of interest. Significance was determined with the Mann–Whitney test, with ns, *, **, ***, and **** representing not significant, $p \leq 0.05$, $p \leq 0.01$, $p \leq 0.001$, and $p \leq 0.0001$.

Figure 3. Changes in Mitochondrial Branching and Networking after Aging Revealed by Serial Block-face Scanning Electron Microscopy. (A) 3D reconstructions showing young and (B) old human skeletal muscle from a transverse point of view. (A’) 3D reconstructions showing young and (B’) old human skeletal muscle from a longitudinal point of view. (C) Sphericity of mitochondria in the young and old groups. (D) The mitochondrial complexity index (MCI), which is analogous to sphericity, was used to compare the young and old groups. (E) Mito-otyping was used to display the diversity of mitochondrial phenotypes, as ordered by volume, to show the mitochondrial distribution in the young and old groups. Each dot represents the average of all mitochondria quantifications in each region of interest. Significance was determined with the Mann–Whitney test, with **** representing $p \leq 0.0001$.

Figure 4. Aging Changes Exercise Parameters Associated with Immune Modulatory Functions. Exercise data from (A–H) females under 50 years old (aged 21–26 years; n = 8), females over 50 years old (aged 60–73 years; n = 15), (A'–H') males under 50 years old (aged 19–35 years; n = 27), and males over 50 years old (aged 63–76 years; n = 12). Blue bars represent young individuals, and purple bars represent older individuals. (A–B) Scatter plots detailing weight and body mass index distribution of females and (A'–B') of young and old individuals, (C–C') walking distances (in meters), and (D–D') VO_2 max values during a walking test among the same groups. (E–F) Scatter box plots for grip strength in kg. (E) Left grip strength and (F) right grip strength for females and (E'–F') males. (G–H) Plots representing localized muscle endurance (G) of the lower body and (H) the upper body across females and (G'–H') males. (I–N) Molecular and physiological measurements from the plasma of male subjects; the full analysis is shown in Supplemental Figure 4. (I) Glycated hemoglobin (A1C) percentage levels in young and old subjects. (J) Glucose concentration levels, presented in milligrams per deciliter (mg/dl), in young and old subjects. (K) Average concentration of hemoglobin in a given volume of packed red blood cells, known as the mean corpuscular hemoglobin (MCH), measured in picograms (pg) for both age groups. (L) Erythrocyte (red blood cell) count measured in millions per cubic millimeter (mm^3) for young and old subjects. (M) Monocyte count, depicted as cells per cubic millimeter (cells/mm^3), for young and old subjects. (N) Band cell (immature white blood cell) count measured in cells/mm^3 for young and old subjects. (O) *In vitro* exercise stimulation in human myotubes with L-lactate and (P) glucose quantification after 4.5 and (Q–R) 24 hours. IL6 mRNA levels, as determined by quantitative PCR, are shown for (S) C2C12 cells, (U) primary myotubes, and (W) human myotubes. FGF21 mRNA levels, as determined by quantitative PCR, are shown for (T) C2C12 cells, (V) primary myotubes, and (X) human myotubes. Each dot represents an individual patient (Supplemental File 2) or experimental run. Significance was determined with the Mann–Whitney test, with **** representing $p \leq 0.0001$.

Figure 5. Mitofusin 2 (MFN2) Expression Changes in Response to Exercise and Aging and Changes in Mitochondrial Morphology. (A) Bar graphs show the mRNA levels, as determined by quantitative PCR, of MFN2 at two distinct time points, 3 months and 2 years, from murine soleus tissue, (B) gastrocnemius tissue, (C) the tibialis, and (D) cardiac tissue. (E) Western blot analysis of MFN2, calreticulin (CALR), and actin protein levels in C2C12 cells and (E') primary myotubes after *in vitro* exercise stimulation at two time intervals, 0 and 4.5 hours. (F–G) Quantitative analysis of lactate and glucose levels in C2C12 cells and (F–G') primary myotubes after *in vitro* exercise stimulation for 4.5 hours. (H–I) Quantitative analysis of lactate and glucose levels in C2C12 cells and (H–I') primary myotubes after *in vitro* exercise stimulation for 24 hours. (J) Quantification of MFN2 protein levels, normalized to actin levels, after 4.5 hours of *in vitro* exercise stimulation in C2C12 cells and (J') primary myotubes. (K) Quantification of CALR protein levels, normalized to actin levels, after 4.5 hours of *in vitro* exercise stimulation in C2C12 cells and (K') primary myotubes. (L–S) Transmission electron microscopy (TEM) images from murine-derived skeletal muscle myotubes highlighting mitochondrial morphology under different conditions: (L–M) control, (N–O) Mitofusin 1 knockout (MFN1 KO), (P–Q) Mitofusin 2 knockout (MFN2 KO), and (R–S) double knockout (DKO). (T–U) Quantitative representation of (T) mitochondrial number, (U) mitochondrial area, and (V) mitochondrial circularity in cells under control, MFN1 KO, and MFN2 KO conditions. (W–Y) Quantitative representation of (W) cristae number, (X) cristae volume, and (Y) cristae surface area in cells under control, MFN1 KO, and MFN2 KO conditions. Intergroup comparisons were performed

using one-way ANOVA with Dunnett's multiple comparisons test *post hoc*. Statistical significance is denoted as ns (not significant), *p < 0.05, **p < 0.01, ***p < 0.001, or ****p < 0.0001.

Figure 6. Comparative Analysis of the Impact of Mitochondrial Assembly Regulatory Factor Knockdown (MARF KD) on Mitochondrial Biogenesis and Cellular Features. (A) Schematic representation of the study organism, highlighting specific anatomical regions of flight muscle. (B) Validation of MARF KD through mRNA fold changes, as determined by quantitative PCR. (C) Visual comparison of wild-type (left) and MARF KD (right) organisms. (D) Fly step quantity changes between wild-type and MARF KD organisms highlight functional differences. (E) Scatter plot of comparing RNA-sequencing reads between wild-type and MARF KD muscles showing differentially expressed genes, with upregulated genes in red and downregulated genes in blue. Select genes are indicated. (F) IPA results for enriched Canonical Pathway terms with an absolute activation Z-score > 2. (G) Heatmap displaying genes related to mitochondrial biogenesis, with gradient colors representing altered expression levels in Marf KD animals compared with controls. The full list of gene names corresponding to FlyBase IDs is available in Supplemental File 3. (H–O) Molecular evaluation of wild-type and MARF KD organisms according to mRNA fold change, as determined by quantitative PCR. (H–J) Mitochondrial dynamic proteins: (H) Marf, (I) OPA1, and (J) DRP1; (K–M) endoplasmic reticulum stress proteins: (K) ATF4, (L) ATF6, and (M) IREI1 3; (N–O) mitochondria–endoplasmic reticulum contact site proteins: (N) GRP75 and (O) VDAC. (P–Q) Transmission electron microscopy images of wild-type flight muscle: (P) longitudinal section and (Q) cross-section. (R–S) Transmission electron microscopy images of MARF KD flight muscle: (R) longitudinal section and (S) cross-section. (T) Quantification of mitochondrial number, (U) mitochondrial area, and (V) circularity index in both conditions. (W) Quantification of cristae volume, (X) cristae surface area, and (Y) cristae score in wild-type and MARF KD mitochondria. (Z–AA) Immunofluorescence images displaying mitochondrial protein localization in wild-type and MARF KD organisms: (Z) Mito-GFP (green) and VDAC (red) with DAPI (blue) nuclear staining and (AA) Mito-GFP (green) and MCJ (red) with DAPI (blue) nuclear staining. (AB) Quantitation of the number of mitochondria per sarcomere in *Drosophila* flight muscle and (AC) aspect ratio (ratio of the major axis to the minor axis). (H–O) Each dot represents an independent experimental run or (T–Y; AB–AC) individual mitochondrial values. Significance was determined with the Mann–Whitney test, with ns, *, **, ***, and **** representing not significant, $p \leq 0.05$, $p \leq 0.01$, $p \leq 0.001$, and $p \leq 0.0001$.

Videos:

Videos 1–4: Behavior and motor function of control *Drosophila* (Videos 1–2) and Marf knockdown organisms (Videos 3–4)

Supplemental Figures:

Supplemental Figure 1: Sex-dependent Differences in Magnetic Resonance Imaging Measurements. (A) Grouped measurements of thigh and femur cross-sectional area (CSA) in males and females. (B) Scatter box plot detailing thigh CSA and (C) femur CSA across young males, young females, older males, and older females. Intra- and inter-sex-dependent differences

during aging are compared. (A) Multiple Mann–Whitney tests with the two-stage step-up method of Benjamini, Krieger, and Yekutieli were used to correct for the false discovery rate. (B–C) Intergroup comparisons were performed using one-way ANOVA with Tukey's multiple comparisons test *post hoc*. Statistical significance is denoted as ns (not significant), *p < 0.05, **p < 0.01, ***p < 0.001, ****p < 0.0001.

Supplemental Figure 2: Heterogeneity in Mitochondrial Quantification in Regions of Interest (ROIs). For each of the three ROIs considered, 250 mitochondria were quantified, for a total of 750 mitochondria in both the young and old human skeletal muscle groups. (A) ROI heterogeneity in mitochondria volume, (B) surface area, (C) perimeter, (D) sphericity, and (E) complexity index in young and old human skeletal muscle.

Supplemental Figure 3: Differences in Exercise Parameters Between Young and Old Humans Across Both Sexes. (A) Chart representing various parameters (weight, height, body mass index (BMI), walking distance, VO_2max, right and left grip strength, and muscle endurance of the upper and lower body) comparing young and old individuals. Blue bars represent young individuals, and purple bars represent older individuals. (B) Scatter box plot detailing weight distribution across young males, young females, older males, and older females for comparison of intra- and inter-sex-dependent differences in aging. (C) Scatter box plot illustrating the distribution of BMI values, (D) walking distances (in meters), and (E) VO_2max values during a walking test among the same groups. (F–G) Scatter box plots for grip strength in kg: (F) left grip strength and (G) right grip strength across the four demographic groups. (H–I) Scatter box plots representing localized muscle endurance (H) of the lower body and (I) the upper body across young males, young females, older males, and older females. (A) Multiple Mann–Whitney tests with the two-stage step-up method of Benjamini, Krieger, and Yekutieli were used to correct for the false discovery rate. (B–I) Intergroup comparisons were performed using one-way ANOVA with Tukey's multiple comparisons test *post hoc*. Statistical significance is denoted as ns (not significant), *p < 0.05, **p < 0.01, ***p < 0.001, ****p < 0.0001.

Supplemental Figure 4: Full Screening of Various Parameters or Biomolecules in the Blood of Older and Young Individuals. The chart displays the full extent of parameters considered when comparing young and older individuals. Multiple Mann–Whitney tests with the two-stage step-up method of Benjamini, Krieger, and Yekutieli were used to correct for the false discovery rate. Statistical significance is denoted as ns (not significant) or * (significant).

Supplementary Figure 5: RNA-sequencing Pathway Analyses Following Marf Knockdown (Marf KD) (A and B) Bubble plots of Gene Set Enrichment Analysis (GSEA) showing enriched cellular components (A) and biological processes (B) impacted by Marf KD compared with the wild-type condition. (C-E) Bubble plots of Ingenuity Pathway Analysis (IPA) results for terms annotated for Diseases or Functions (C), Upstream Regulators (D), and Canonical Pathways (E). Data for (E) is the same as in main Figure 6E but is expanded here to include additional terms having an absolute activation Z-score > 1.5. For all panels, enrichment and activation Z-scores between -2 and +2 are indicated by a gray box and are considered insignificant. The color of each term symbol reflects the -Log p-value or false discovery rate (FDR) as indicated by the color scale.

Supplementary Figure 6: Heatmap Analysis of Pathways Altered Following Marf Knockdown (Marf KD). Heatmaps of altered expression of proteins associated with (A)

mitophagy, (B) mammalian target of rapamycin (mTOR), (C) sphingolipid signaling, and (D) DNA synthesis. The full list of gene names corresponding to FlyBase IDs is available in Supplemental File 3. The color scale on the right side represents expression values, with red indicating upregulation and green indicating downregulation.

Supplemental Files:

Supplemental File 1. Full magnetic resonance imaging parameters, including patient age.

Supplemental File 2. Full exercise parameters, including patient age and weight.

Supplemental File 3. Orthologs of FlyBase ID names and fly gene names.

Supplemental File 4. Significant differentially expressed genes with GSEA and IPA analysis results.

Figure 1

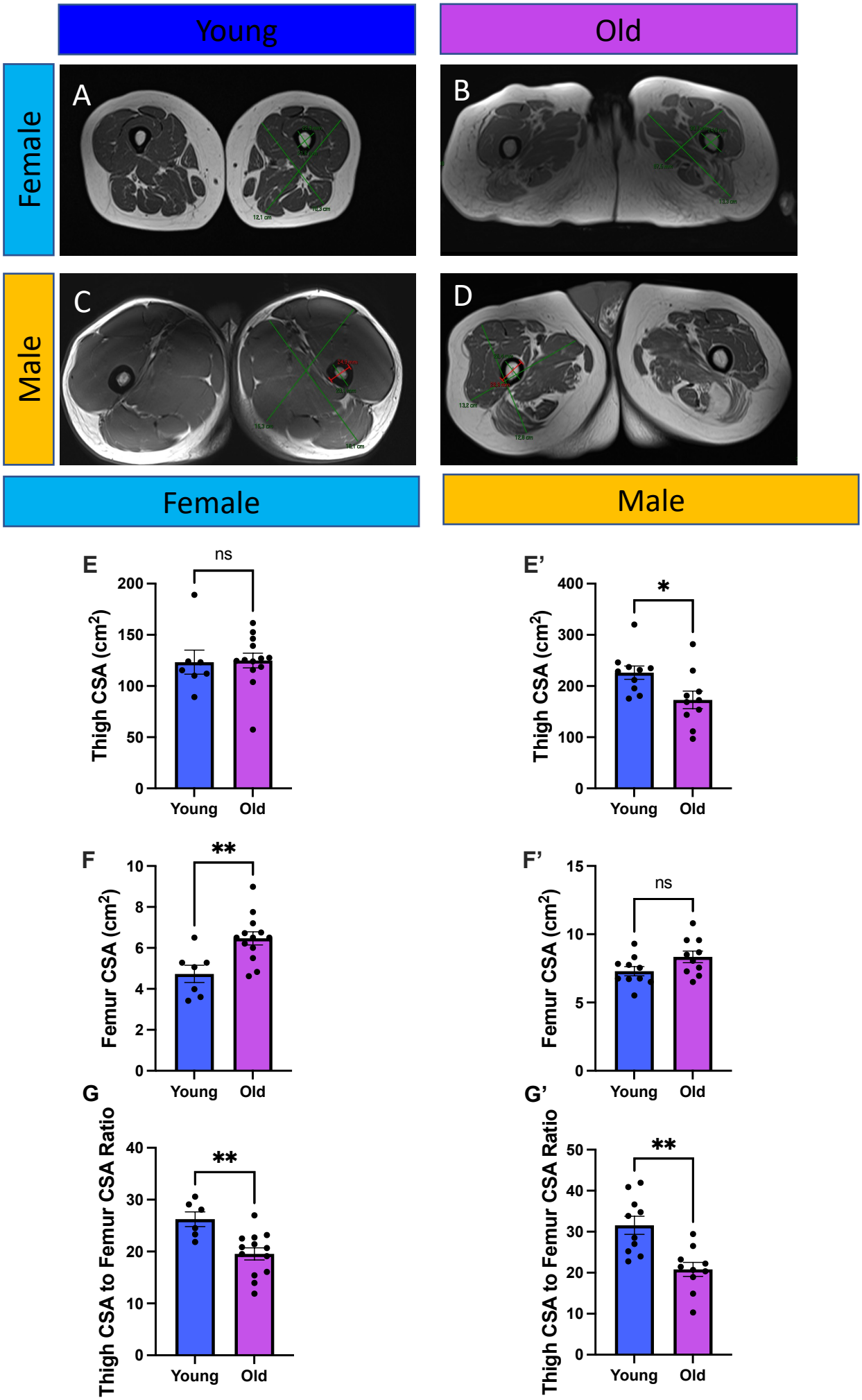
Young
Old
Female
Male
A
B
C
D
Female
Male
E
ns
Thigh CSA (cm2)
200
150
100
50
0
Young
Old
E'
*
Thigh CSA (cm2)
400
300
200
100
0
Young
Old
F
**
Femur CSA (cm2)
10
8
6
4
2
0
Young
Old
F'
ns
Femur CSA (cm2)
15
10
5
0
Young
Old
G
**
Thigh CSA to Femur CSA Ratio
40
30
20
10
0
Young
Old
G'
**
Thigh CSA to Femur CSA Ratio
50
40
30
20
10
0
Young
Old

Figure 2

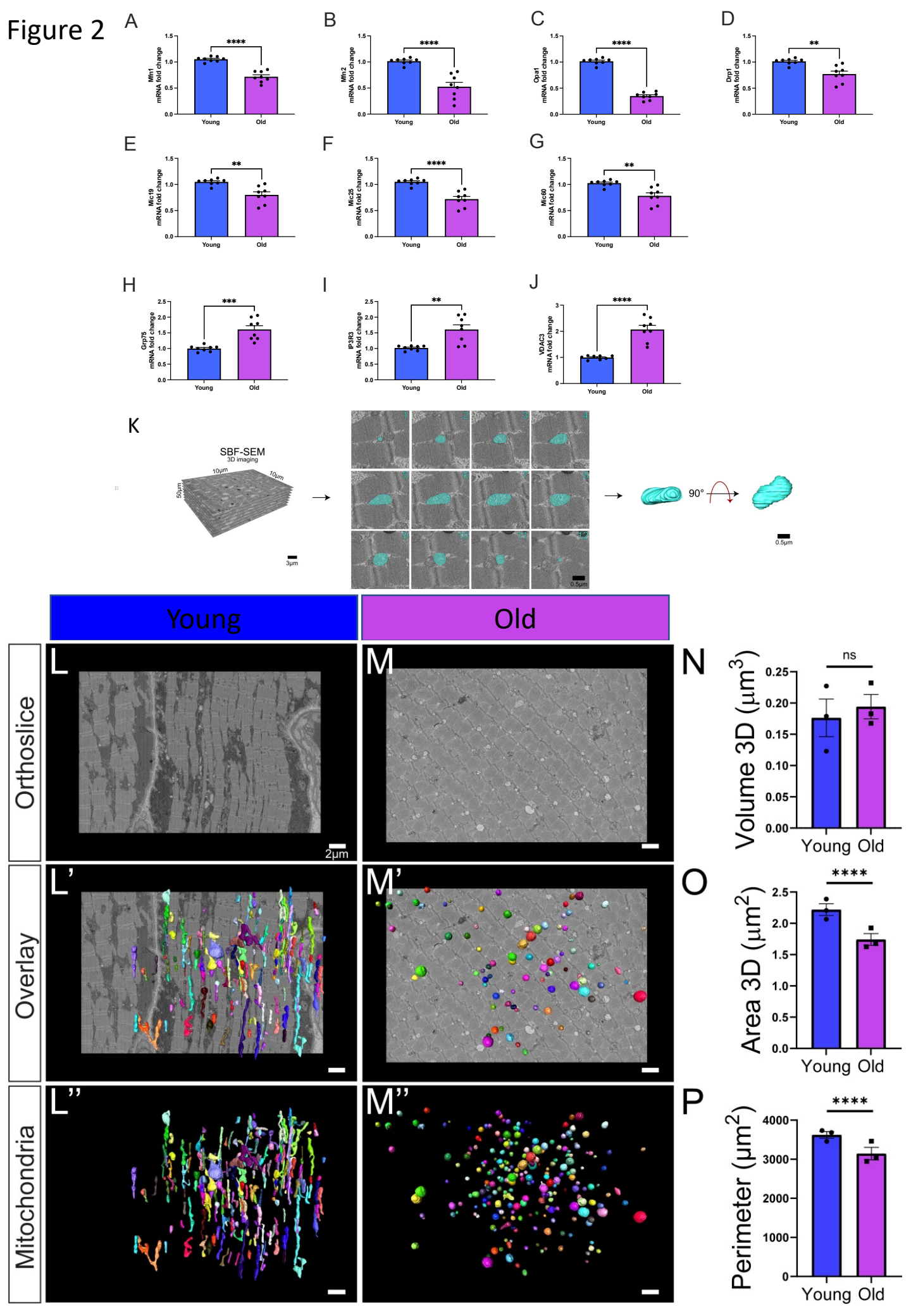
A
Mfn1 mRNA fold change
****
Young
Old
B
Mfn2 mRNA fold change
****
C
Opa1 mRNA fold change
****
D
Drp1 mRNA fold change
**
E
Mic19 mRNA fold change
**
F
Mic25 mRNA fold change
****
G
Mic60 mRNA fold change
**
H
Grp75 mRNA fold change
***
I
IP3R3 mRNA fold change
**
J
VDAC3 mRNA fold change
****
K
SBF-SEM
3D imaging
10µm
10µm
50µm
3µm
0.5µm
90°
0.5µm
Young
Old
Orthoslice
Overlay
Mitochondria
L
M
N
L'
M'
O
L''
M''
P
2µm
ns
Volume 3D (µm3)
Area 3D (µm2)
Perimeter (µm2)

Figure 3

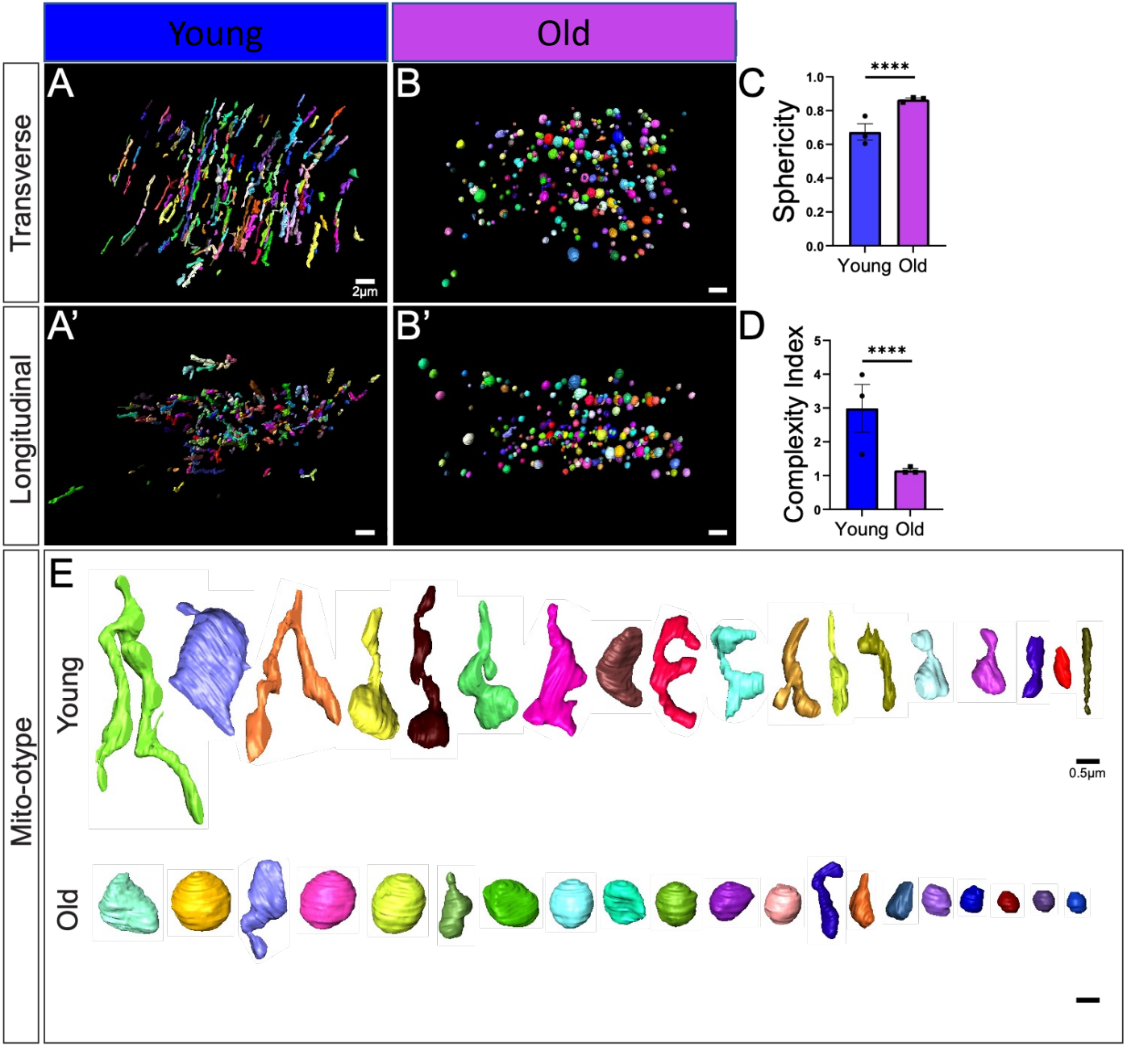
Young
Old
Transverse
Longitudinal
Mito-otype
A
B
A'
B'
C
D
E
2µm
Sphericity
Complexity Index
****
****
Young
Old
0.5µm

Figure 4

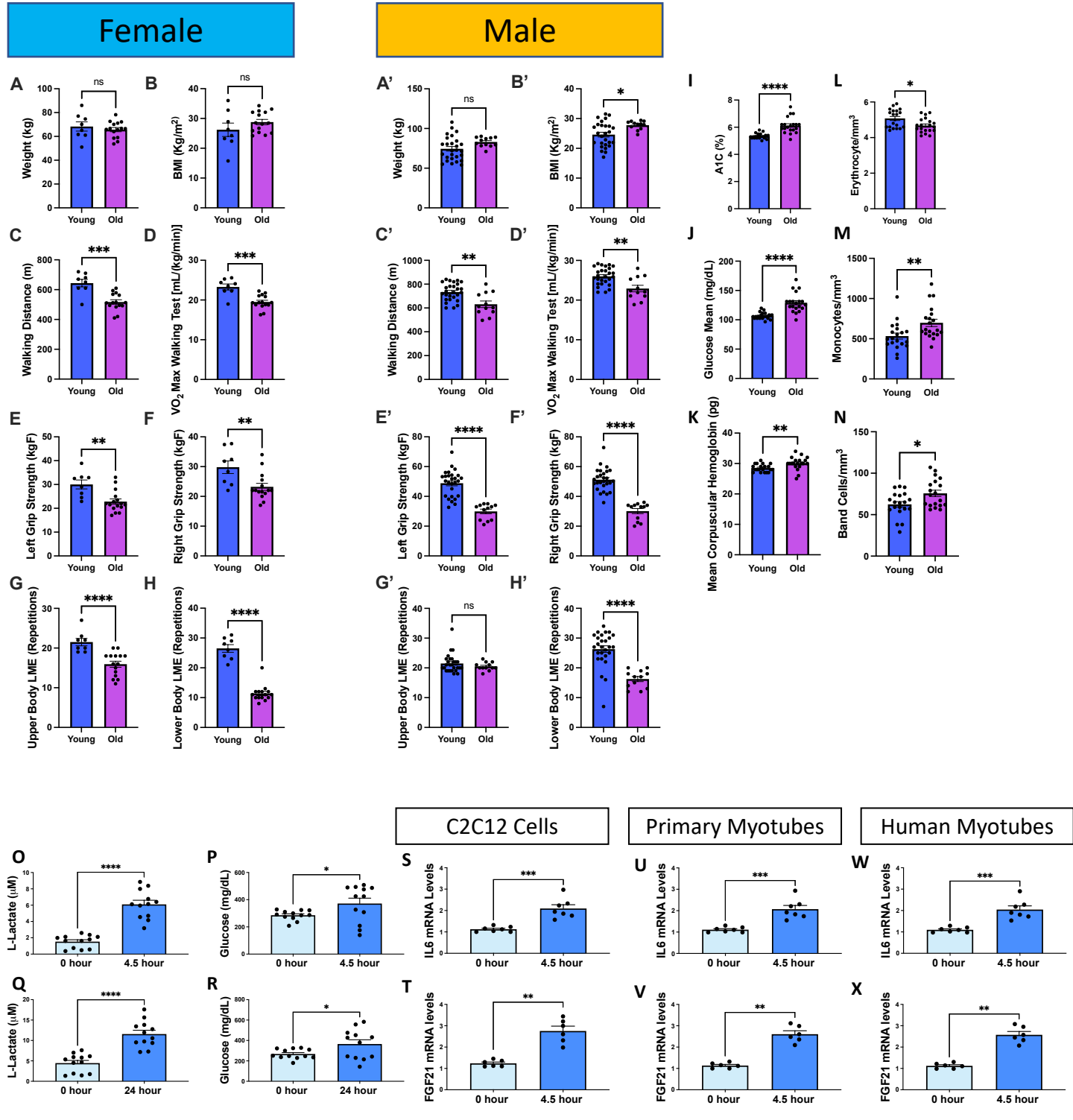
Female
Male
A
Weight (kg)
ns
B
BMI (Kg/m²)
ns
A'
Weight (kg)
ns
B'
BMI (Kg/m²)
*
I
A1C (%)
****
L
Erythrocyte/mm³
*
C
Walking Distance (m)
***
D
VO₂ Max Walking Test [mL/(kg/min)]
***
C'
Walking Distance (m)
**
D'
VO₂ Max Walking Test [mL/(kg/min)]
**
J
Glucose Mean (mg/dL)
****
M
Monocytes/mm³
**
E
Left Grip Strength (kgF)
**
F
Right Grip Strength (kgF)
**
E'
Left Grip Strength (kgF)
****
F'
Right Grip Strength (kgF)
****
K
Mean Corpuscular Hemoglobin (pg)
**
N
Band Cells/mm³
*
G
Upper Body LME (Repetitions)
****
H
Lower Body LME (Repetitions)
****
G'
Upper Body LME (Repetitions)
ns
H'
Lower Body LME (Repetitions)
****
Young
Old
C2C12 Cells
Primary Myotubes
Human Myotubes
O
L-Lactate (μM)
****
P
Glucose (mg/dL)
*
S
IL6 mRNA Levels
***
U
IL6 mRNA Levels
***
W
IL6 mRNA Levels
***
Q
L-Lactate (μM)
****
R
Glucose (mg/dL)
*
T
FGF21 mRNA levels
**
V
FGF21 mRNA levels
**
X
FGF21 mRNA levels
**
0 hour
4.5 hour
24 hour

Figure 5

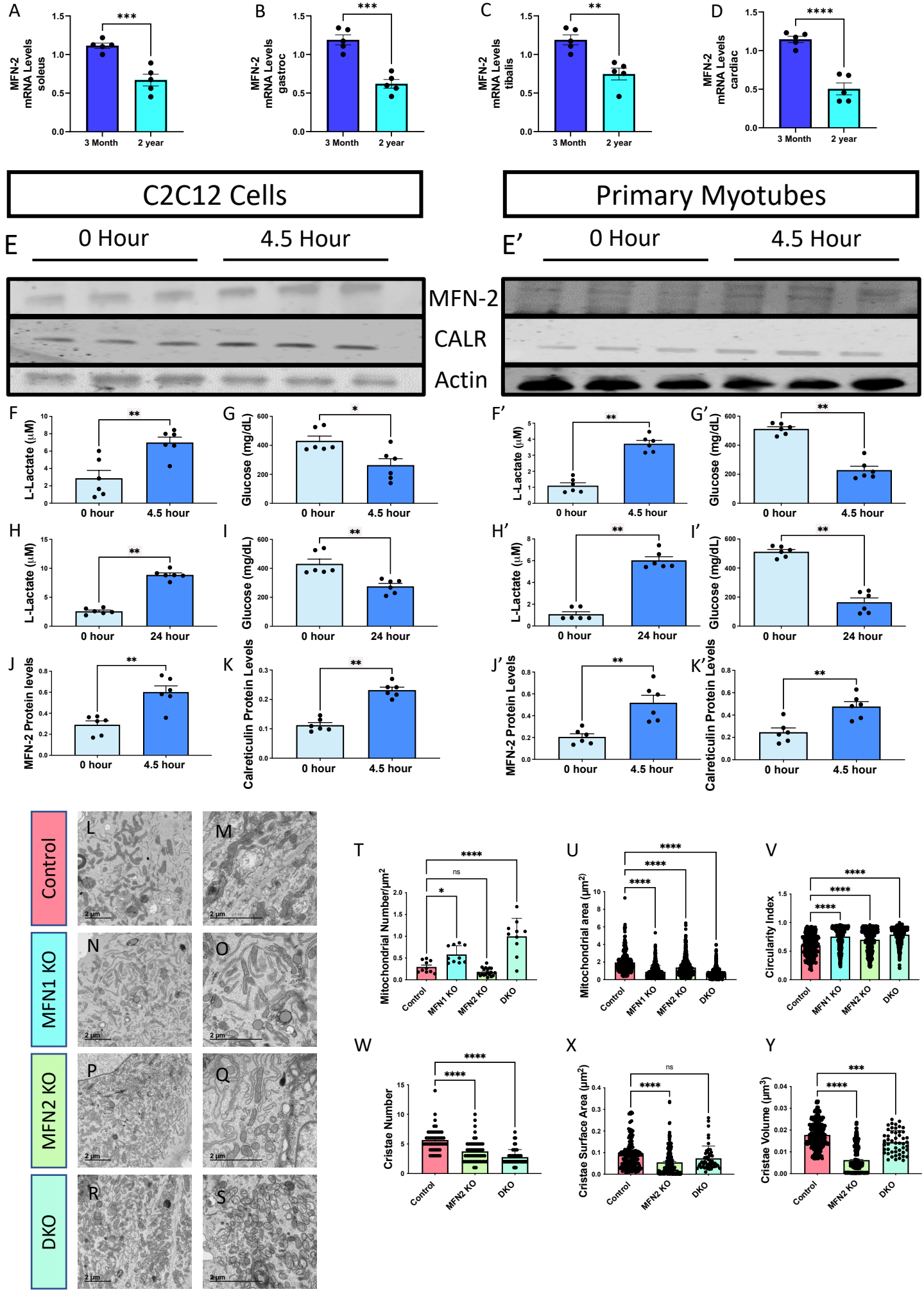
A
MFN-2 mRNA Levels soleus
3 Month
2 year
B
MFN-2 mRNA Levels gastroc
C
MFN-2 mRNA Levels tibalis
D
MFN-2 mRNA Levels cardiac
C2C12 Cells
Primary Myotubes
E
0 Hour
4.5 Hour
E'
MFN-2
CALR
Actin
F
L-Lactate (μM)
G
Glucose (mg/dL)
F'
G'
H
24 hour
I
H'
I'
J
MFN-2 Protein levels
K
Calreticulin Protein Levels
J'
K'
Control
MFN1 KO
MFN2 KO
DKO
L
M
N
O
P
Q
R
S
T
Mitochondrial Number/μm²
U
Mitochondrial area (μm²)
V
Circularity Index
W
Cristae Number
X
Cristae Surface Area (μm²)
Y
Cristae Volume (μm³)

Figure 6

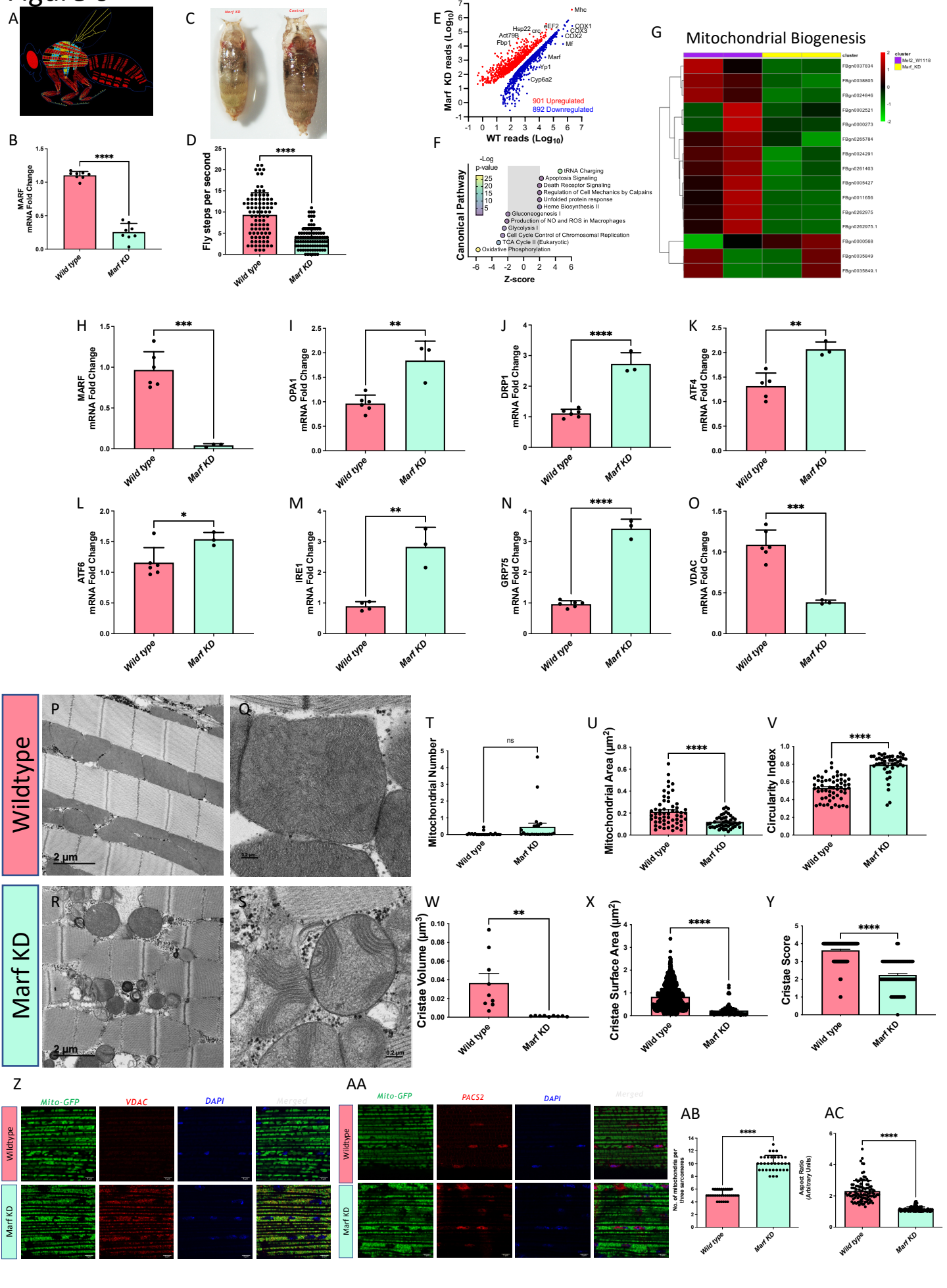
A
B
MARF mRNA Fold Change
****
Wild type
Marf KD
C
Marf KD
Control
D
Fly steps per second
****
E
Marf KD reads (Log10)
WT reads (Log10)
Mhc
COX1
COX3
COX2
Mf
Marf
Yp1
Cyp6a2
eEF2
crc
Hsp22
Act79B
Fbp1
901 Upregulated
892 Downregulated
F
Canonical Pathway
-Log p-value
tRNA Charging
Apoptosis Signaling
Death Receptor Signaling
Regulation of Cell Mechanics by Calpains
Unfolded protein response
Heme Biosynthesis II
Gluconeogenesis I
Production of NO and ROS in Macrophages
Glycolysis I
Cell Cycle Control of Chromosomal Replication
TCA Cycle II (Eukaryotic)
Oxidative Phosphorylation
Z-score
G
Mitochondrial Biogenesis
cluster
Mef2_W1118
Marf_KD
FBgn0037834
FBgn0038805
FBgn0024846
FBgn0002521
FBgn0000273
FBgn0265784
FBgn0024291
FBgn0261403
FBgn0005427
FBgn0011656
FBgn0262975
FBgn0262975.1
FBgn0000568
FBgn0035849
FBgn0035849.1
H
MARF mRNA Fold Change
***
I
OPA1 mRNA Fold Change
**
J
DRP1 mRNA Fold Change
****
K
ATF4 mRNA Fold Change
**
L
ATF6 mRNA Fold Change
*
M
IRE1 mRNA Fold Change
**
N
GRP75 mRNA Fold Change
****
O
VDAC mRNA Fold Change
***
Wild type
Marf KD
Wildtype
Marf KD
P
Q
R
S
2 µm
0.2 µm
T
Mitochondrial Number
ns
U
Mitochondrial Area (µm²)
****
V
Circularity Index
****
W
Cristae Volume (µm³)
**
X
Cristae Surface Area (µm²)
****
Y
Cristae Score
****
Z
Mito-GFP
VDAC
DAPI
Merged
AA
PACS2
AB
No. of mitochondria per three sarcomeres
AC
Aspect Ratio (Arbitrary Units)